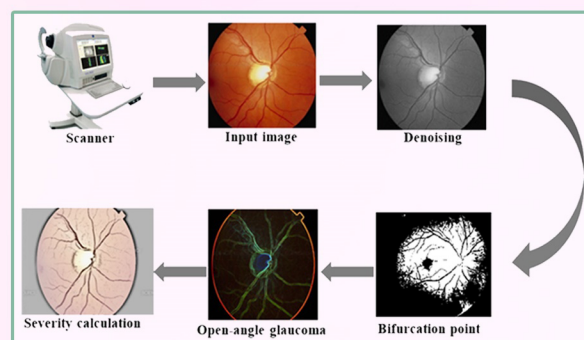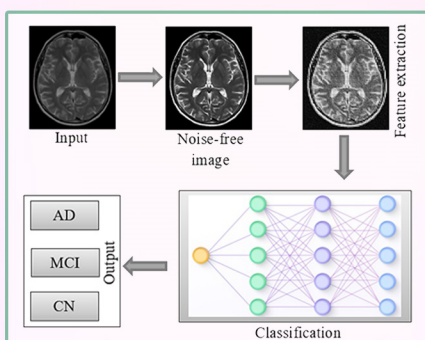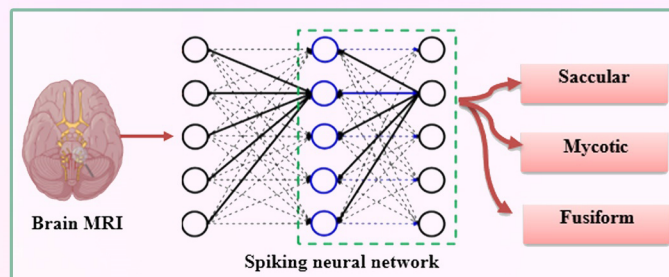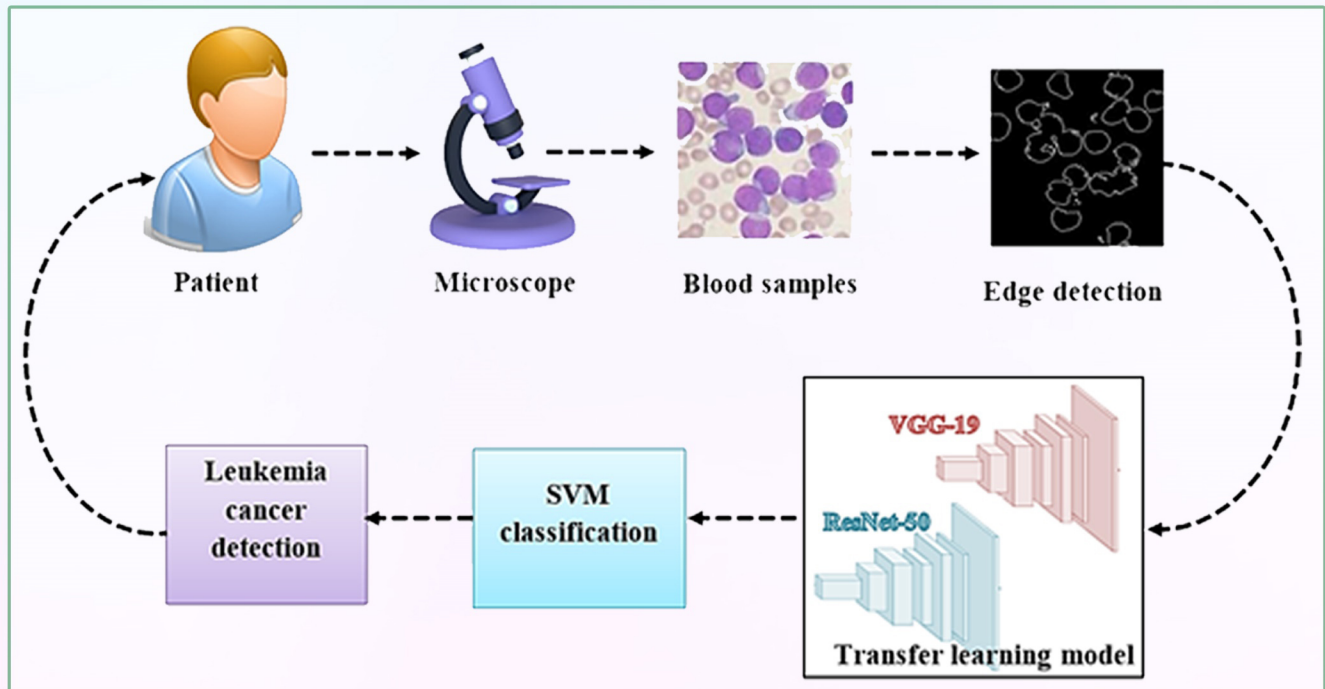KITS PRESS
For the Research

IJCBE

ISSN : XXXX-XXXX

International Journal of Current Biomedical Engineering
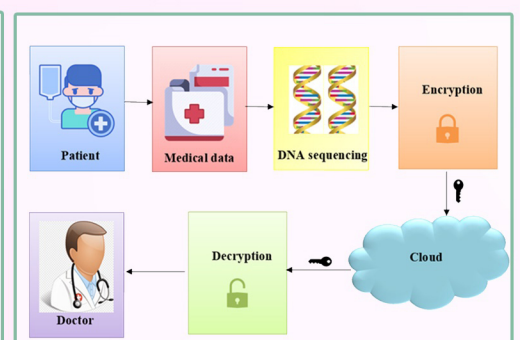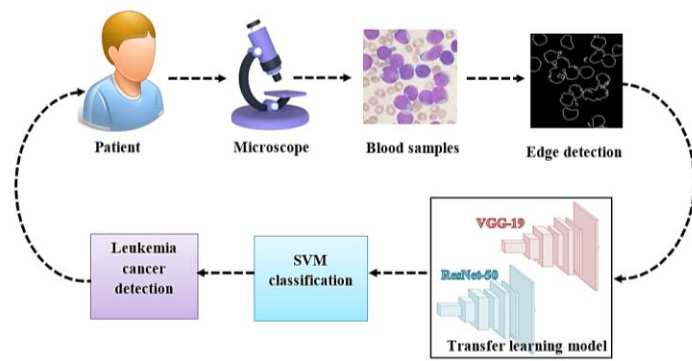
International Journal of Current Bio-Medical Engineering (IJCBE)

1. LEUKEMIA CLASSIFICATION USING A FUSION OF TRANSFER LEARNING AND SUPPORT VECTOR MACHINE

P. G. SreeLekshmi, P. Linu Babu, P. Josephin Shermila

Abstract – Leukemia is a malignancy that originates in the bone marrows and it is characterised by aberrant white blood cell growth. Artificial intelligence has flourished in recent years across all scientific disciplines. The accuracy of predicting the initial severity of this infection using artificial intelligence in medical research has increased. The proposed model uses transfer leaning approach with VGG-19, and ResNet-50. The input images are pre-processed by weighted distribution and gamma correction techniques; from this the edges are detected by the Sobel edge detector. The structural features are extracted by the deep neural networks and acquired as feature sets. These feature sets are fused by least absolute shrinkage and selection operator (LASSO) and the support vector machine (SVM) is utilized to categor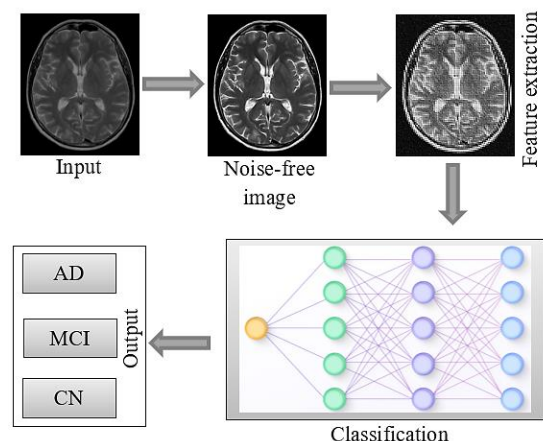ize the four types of leukemia and healthy. When compared to the results produced by the existing deep neural networks, the proposed approach produces the most precise and effective outcomes. This model yields the accuracy rate of 99.08% and 99.02% for the classification of leukemia.

Keywords – *Leukemia, Weighted distribution, Transfer learning, Feature fusion, Classification.*

2. ALZHEIMER DISEASE DETECTION VIA DEEP LEARNING BASED SHUFFLE NETWORK

D. S. Dakshina, Della Reasa Valiaveetil, A. Bindhu

Abstract – Alzheimer's disease (AD) is a progressive neuro de-generative ailment that decimates the brain memory. The early stage of Alzheimer's is mild cognitive impairment (MCI) and it is hardly possible to diagnosis. Artificial intelligence (AI) has proliferated in recent years across all scientific disciplines. The early detection of AD is now more accurate and precise thanks to the application of AI in medicine. In the proposed study, introducing a novel technique named ShuffleNet for prognosticating dementia, which is intended to assist doctors in diagnosing AD. Magnetic resonance imaging (MRI) was collected from Alzheimer's disease Neuroimaging Initiative-3 (ADNI-3) and pre-processed using Histogram Equalization (HE). ShuffleNet a deep neural network combined with the leaky ReLU was used for extracting the surface features from brain MRI. Finally, the proposed system's effectiveness was demonstrated by the correct classification that was acquired using the multi-layered perceptron (MLP) classifier. When compared to CNN's current networks, the suggested model's findings are the best and most accurate. This model yields the sensitivity range of 98.22%, specificity range of 98.75% and accuracy rate of 99.72% respectively with the minimal computational cost.
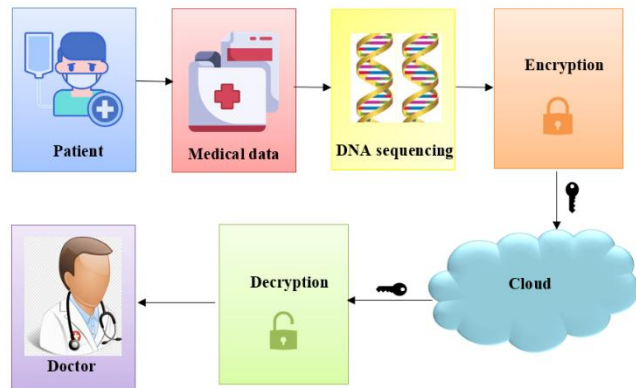
Keywords – Alzheimer Disease, Artificial Intelligence, ShuffleNet, Learning, Brain Magnetic Resonance Images.

3. SECURE STORAGE OF LUNG BRAIN MULTI-MODAL MEDICAL IMAGES USING DNA HOMOMORPHIC ENCRYPTION

S. Gnana Sophia, K. K. Thanammal, S. S. Sujatha

Abstract – Protecting the medical data on the online platform for transmitting data is a simple and demanding task. In the modern world, various methods are used to safeguard the digital image such as cryptography, watermarking, and steganography. These methods are used for protecting digital images in order to achieve security objectives such as confidentiality, reliability, and usefulness. In the proposed method, the medical images are encrypted and stored in cloud using DNA Homomorphic Encryption (DNA-HE) algorithm. The key is generated using Rider Optimization Technique to ensure security. It acts as double encryption technique. Homomorphic encryption is an authentication approach that allows one to perform observations on encrypted data by decrypting it. In DNA Homomorphic Encryption algorithm, the input data will be a DNA sequence. The same procedure is used to decrypt the encrypted data. Performance of the proposed technique is evaluated using a number of factors, including execution, encryption, and decryption times.
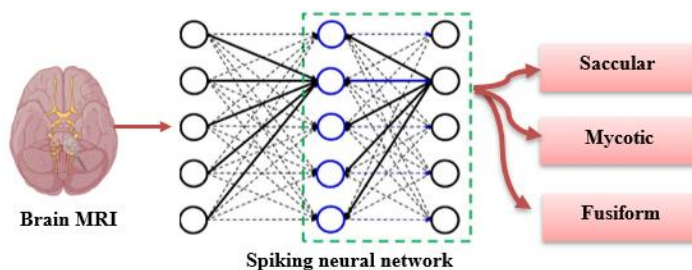
Keywords– DNA Homomorphic algorithm, Rider Optimization algorithm, Encrypting medical images, Decryption.

4. BRAIN ANEURYSM DETECTION VIA FIREFLY OPTIMIZED SPIKING NEURAL NETWORK

A. Jegatheesh, N. Kopperundevi, M. Anlin Sahaya Infant Tinu

Abstract – Aneurysms in the brain occur often; the frequency is around 4%. The mass effect is mostly responsible for the symptoms of unruptured aneurysms. The actual risk arises if the aneurysm bursts and results in a subarachnoid haemorrhage, though. The majority of aneurysms are asymptomatic and do not burst, although even minor aneurysms can do so due to the unpredictable growth of aneurysms. Imaging methods including intra-arterial digital subtraction angiography, computed tomography angiography, and magnetic resonance angiography are used to diagnose and track intracranial aneurysms. In this paper, a deep learning approach is proposed to detect and classify the brain aneurysm. Initially, the MRI images are skull stripped and the images augmented and reduce the noise using Kalman filter in the pre-process phase. The segmentation can be done by the firefly optimization algorithm. The segment nodules are classified into three classes by using the spiking neural network. The proposed model achieves the highest level of classification accuracy, which is 99.80%. As a result, when compared to other models currently in use, classification using BSF yields results that are much higher in efficiency and accuracy.
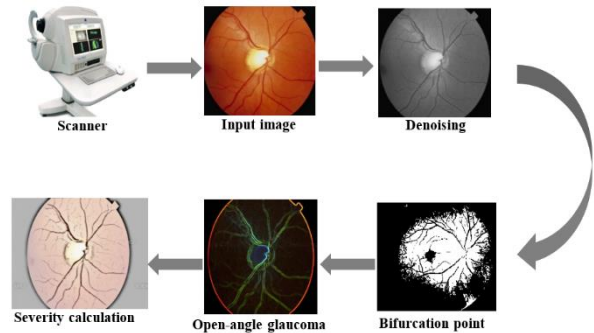
Keywords – Brain aneurysm, firefly optimization algorithm, Kalman filter, spiking neural network.

5. PRIMARY OPEN-ANGLE GLAUCOMA SEVERITY PREDICTION USING DEEP LEARNING TECHNIQUE

Dr. A. Prasanth, Dr. N. Muthukumaran

Abstract – Glaucoma is a neuro optical disorder that lead to blindness over a period of time. In recent years, studies have revealed that diabetic patients are more common victims of glaucoma. The present research aims to investigate the relationships between intraocular pressure (IOP), refractive error, and primary open-angle glaucoma (POAG) in the wheatish population. Population-based research provide important information on the prevalence and hazards for glaucoma, such eye refractive defects. At low IOP stages, the correlation between glaucoma and myopia is strong, and it gradually decreases as IOP rises. A Deep learning tool is developed to analyze the severity of glaucoma using fundus image. According to this research, the association between IOP and glaucoma is strong at low mean values of 15 ± 3.23 level and gradually weakens as IOP increases in the wheatish population, reaching 17.59 ± 3.33 for PACG, 18.85 ± 1.20 for POAG, 18.59 ± 2.52 for PIGM, and 19.12 ± 1.42 for OH. With increasing IOP, the glaucoma image in myopic eyes degraded, and no correlation with IOP ≥35 mmHg has been found.

RESEARCH ARTICLE

LEUKEMIA CLASSIFICATION USING A FUSION OF TRANSFER LEARNING AND SUPPORT VECTOR MACHINE

P. G. Sreelekshmi[1, *], P. Linu Babu[2] and P. Josephin Shermila[3]

[1]Lecturer in Computer science, Dept- BCA, University Institute of Technology Malayinkeezhu, University of Kerala, University of Kerala Senate House Campus, Palayam, Thiruvananthapuram, Kerala, India.
[2]Ph.D Scholar, Veltech Rangarajan Dr. Sagunthala R & D Institute of Science and Technology, Chennai, India
[3]Associate Professor, Department of Artificial Intelligence and Data Science, R. M. K. College of Engineering and Technology, Chennai, Tamil Nadu, India.

Corresponding e-mail: sreelekshmi1916@gmail.com

Abstract – Leukemia is a malignancy that originates in the bone marrows and it is characterised by aberrant white blood cell growth. Artificial intelligence has flourished in recent years across all scientific disciplines. The accuracy of predicting the initial severity of this infection using artificial intelligence in medical research has increased. The proposed model uses transfer leaning approach with VGG-19, and ResNet-50. The input images are pre-processed by weighted distribution and gamma correction techniques; from this the edges are detected by the Sobel edge detector. The structural features are extracted by the deep neural networks and acquired as feature sets. These feature sets are fused by least absolute shrinkage and selection operator (LASSO) and the support vector machine (SVM) is utilized to categorize the four types of leukemia and healthy. When compared to the results produced by the existing deep neural networks, the proposed approach produces the most precise and effective outcomes. This model yields the accuracy rate of 99.08% and 99.02% for the classification of leukemia.

Keywords – Leukemia, Weighted distribution, Transfer learning, Feature fusion, Classification

1. INTRODUCTION

Leukemia is the frequently known cancer that begins in white blood cells (WBCs), although it can also spread in other types of blood cells and bone marrows [1]. The major categorization of leukaemia is performed in terms of whether it is acute (quickly increasing) or chronic (slowly growing). Similarly, it also begins in myeloid or lymphoid cells affects the blood cells of an individual. In the recent scenario nearly 9,500 peoples were affected by leukemia, according to the survey of GLOBOCAN. The major symptoms of leukemia [5,7] are fatigue, recurrent infections, weight loss, and easy bleeding or bruising are all signs of quickly developing kinds of leukaemia. The leukemia is classified as acute or chronic based on the cell immature growth and the types of the cancer. The first type is acute lymphocytic leukemia (ALL), it commonly affects the children than the other [10]. The

second type is acute myeloid leukemia (AML), it commonly affects the people younger than 20 years. The next categories are chronic lymphocytic leukemia (CLL) and chronic myelogenous leukemia (CML), both affects the older adults. The figure.1 depicts the forms of leukemia.
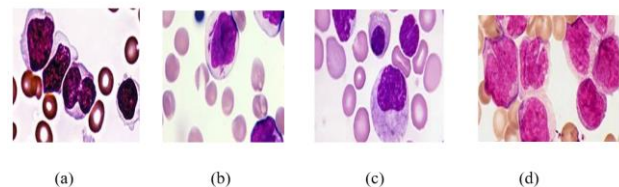
Figure 1. Microscopic view of leukemia types (a) ALL (b) AML (c) CLL and (d) CML

The early detection and diagnosis could help patients minimize expense on therapy, enhance their chances of recovery, and then even survive longer. One of most common tests for detecting leukemia is the smear test [11]. Blood samples are obtained and subjected to various tests in order to predict leukemia. Furthermore, manual diagnoses are inherently incorrect since they require more time and are susceptible to the inter-observer discrepancies. [13-15]. The development of low-cost and autonomous systems that can distinguishes the normal and abnormal blood cells without any human intervention. Several classic computer-aided technologies employ image processing with machine learning and deep learning approaches, [16-20] which often include numerous phases namely pre-processing, segmenting, extracting the features, and classifications. Both machine learning and deep learning approach is more time consuming to overwhelm this issue [21-23] the proposed model uses transfer learning [24-27]. As a consequence, rather of designing deep neural networks from the scratch, employ the principle of transfer learning [28], in which the neural networks that has been successful in addressing one

issue is optimized to resolve others. In this paper transfer learning is used that combines with two deep neural networks namely VGG-19, and ResNet-50 is used for feature extraction. The relevant features are selected by LASSO (Least absolute shrinkage and selection operator) and then the features are fused. SVM (support vector machine) is used to classify the four types of leukemia with high accuracy rate and low cost of computation [29-32].

The rest of the work is spilted into the five sections. The linked works are succinctly explained in Section II. In Section III, the suggested methodology is described. The performance results and their analysis are reported in section IV. The conclusion is provided in Section V.

2. LITERATURE SURVEY

Researchers recently proposed a number of deep learning algorithms, mostly to increase the categorization accuracy of blood cell images. In 2021 Shaheen M. *et al.* [1] had devised the prediction of Acute Myeloid Leukemia (AML) by deep learning algorithms like AlexNet and Lenet-5 models and compared the performance of these both models. The datasets were derived from Acevedo et al. publicly available microscopic peripheral blood samples. When compare both performance Lenet-5 model reaches low accuracy. But, AlexNet reaches high accuracy and detect only AML.

In 2020 Das, *et al.* [2] had developed a GLCM (gray level co-occurrence matrix) and GLRLM (gray level run length matrix) approaches are employed for extracting the characteristics of cells and detect ALL. The datasets were taken by ALL Image Database. SVM is used to classify the WBCs. CLAHE (contrast-limited adaptive histogram equalization) is employ to upgrade the sample qualities. But, SVM takes more time for training the large datasets.

In 2020 Kumar D *et al.,* [3] had proposed a DCNN (dense convolutional neural network) framework to categorize the two types of leukemia namely ALL (acute lymphoblastic leukemia) and MM (multiple myeloma). The datasets had been collected from SMS Spam research. Here, data augmentation introduced two processes, first one is rotating the images corresponding to certain degrees and second one is upgrading only the edges or boundaries of the original image. Uni-variate feature selection had been introduced and selects the features based on univariate statistical tests and its computational rate is high.

In 2019, Tammina, S.,[4] suggested a technique of transfer learning for repurposing previously learned model information for a new task. Classification, regression, and clustering issues can all benefit from transfer learning. Pre-trained InceptionV1, InceptionV2, VGG-16 was trained on ImageNet, that have wide range of image classes. The result illustrates that the introduced model acquires high accuracy than the other models.

In 2018, Cao, G., *et al.,* [5] suggested a technique where the gamma correction controlled by shortened CDF is utilised to improve the dimmed images, while the unique method of negative samples was used to realise CE of the bright ones. The proposed method's algorithm complexity is assessed. Extensive qualitative and quantitative testing demonstrates that suggested strategy provides better or comparable enhancing benefits than earlier strategies.

In 2016, Rahman, S., *et al*., [6] had proposed an AGC technique (adaptive gamma correction) to properly increase the quality of the images, with the attributes of AGC being modified dynamic information based on the input images. An extensive trial, as well as qualitative and quantitative assessments, reveals that the concert of AGC is high than other existing approaches. AGC offers the most satisfactory contrast increases in diverse lighting circumstances when compared to other existing enhancement algorithms.

In 2019, Veluchamy, M. and Subramani, B., [7] presented an Adaptive Gamma Correction with Weighted Histogram Distribution (AGCWHD) approach to increase contrast while keeping original colour and deeper information of the input images. To assess the performance of the suggested technique, experiments are carried out and assessed on 500 TID 2008 benchmark photos. When compared to the existing procedures, experimental findings showed that the suggested methodology created extraordinarily high-quality images.

In 2020, Loey, M., *et al.,* [8] had proposed a method that employs transfer learning technique to diagnosis leukaemia, that includes two automatic classification algorithms based on the blood microscopic examination images, instead of using earlier strategies that have severe disadvantages. Blood microscopic pictures are denoised in the primary technique, and then characteristics are extracted via deep CNN. The result shows that the proposed model recognizes leukaemia in more efficient manner than other models.

In 2019 Ahmed N. *et al.* [9] had proposed CNN is used to classify the subtypes of leukemia like ALL, AML, CLL, and CML. The datasets are picking up by the two publicly available leukemia datasets are ALL image database and ASH image bank. There are various image transformation techniques are applied. The feature extraction phase is carried out in convolution and pooling layer. SGD and Adam optimizers are applied. But, Stochastic Gradient Descent (GCD) makes continuous informs with a huge change, causing the objective function to differ significantly.

In 2018 Shafique.S. and Tehsin.S., [10] had proposed a AlexNet to ALL in an automatic manner and classify its subtypes. The images were taken by public available datasets and four datasets had been selected as different colours. In data augmentation technique, image rotation and mirroring had been feed to increase the training data. For the total datasets, ALL detection accuracy was good but, the classification of subtype's accuracy was lower than the RGB image datasets.

From this study various deep learning and machine learning methods are comfortable to get high accuracy. In this proposed system, transfer learning that integrates VGG-19 and ResNet-50 for extracting the features and the classification of leukemia is performed by support vector machine (SVM) to acquire better accuracy and with low computational rate.
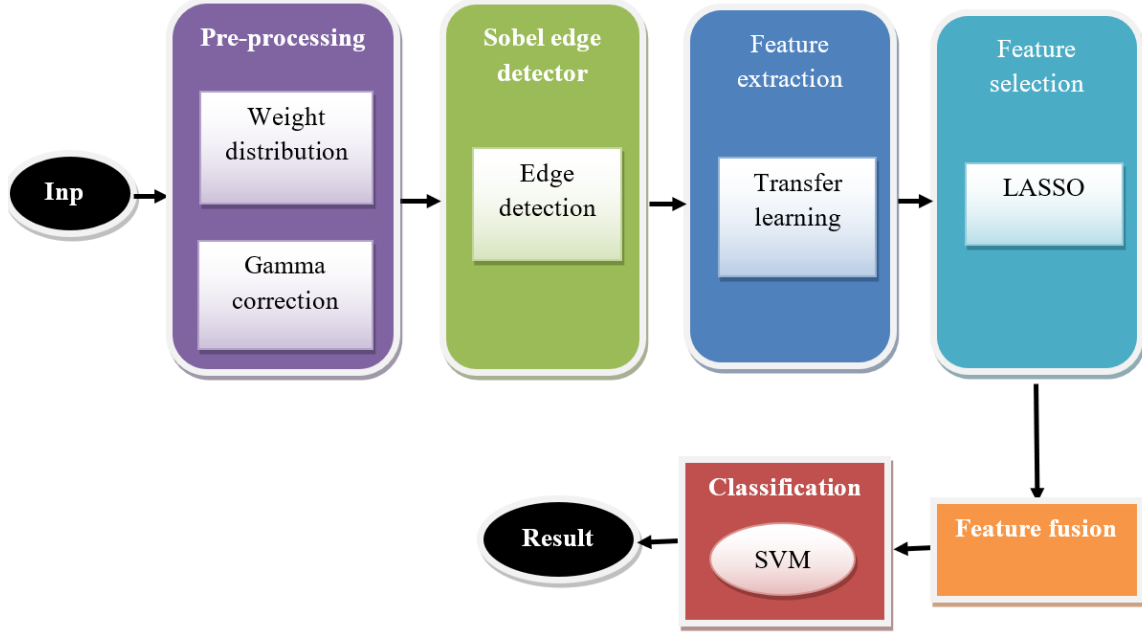
3.   PROPOSED METHOD

Figure 2. Visualization of the proposed approach

3.1. Dataset acquisition

In this study the blood sample images are taken from the commonly available two dataset library namely ASH image bank and ALL-IDB. Four types of leukemia images with size of 2560x1920 in BMP forms constitute this dataset. The collective formats are intended to tune the proposed method to decide the types of leukemia acute and chronic. The acute categories are acute lymphocytic leukemia (ALL) and acute myeloid leukemia (AML). The chronic categories are chronic lymphocytic leukemia (CLL) and chronic myelogenous leukemia (CML),

3.2. Image pre-processing

Pre-processing is an initial step for lessening the noise and improving the subtle variations of medical images. The microscopic blood images are first changed into an RGB colour as input to the model, and then a variety of processes are performed in this stage. To compensate the loss of the datasets, data augmentation is used. The inputs are rotated along the X and Y axes, the interval randomly selecting values. The indication process reflects images all along the vertical axis. At last, with randomly rotating the values that are limited by the intervals, the inputs are twisted right or left during the rotation procedure.

3.3. Weighted Distribution

A weighted distribution is used to ensure that image regions with a high probability do not become highly enhanced, and image regions with a lower probability do not become under-enhanced, with no loss of critical visual features. This input image is altered such that less frequent levels have higher probability or weights. The formula for calculating weighted input is:

$$pdf_w(l) = pdf_{max}(pdf(l) - \frac{pdf_{min}}{pdf_{max}} - pdf_{min})^a \qquad (1)$$

Then modified cumulative density function is derived as,

$$cdf_w(l) = \sum_{l=0}^{lmax} pdf_w(l) / \sum pdf_w \qquad (2)$$

Where,

$$\sum pdf_w = \sum_{l=0}^{lmax} pdf_w(l) \qquad (3)$$

Where α is the adjusted factor, pdf_{max} is the largest probability distribution function and pdf_{min} is the smallest probability distribution function of statistical histogram.

| (a) | (b) |
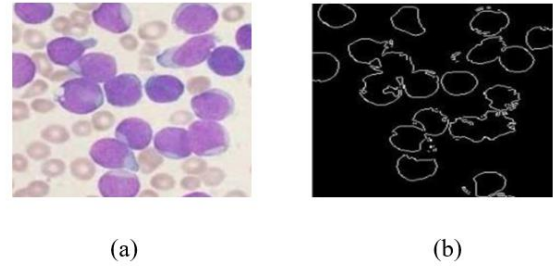
Figure 3. Samples of (a) pre-processed image and (b) after edge detection image

3.4. Gamma Correction

The gamma correction is applied after the weighted distribution is mapped. The normalised cumulative density function (cdf) is used to apply gamma correction in this approach and it is carried out as follows,

$$T(l) = l_{max}(l/l_{max})^\gamma = l_{max}(l/l_{max})^{l-cdf(l)} \qquad (4)$$

Where, the gamma equation is calculated as:

$$\gamma = l - cdf_w(l) \qquad (5)$$

where the distribution function is indicated as cdf_w, the max signifies the exploiting operator and l defines the pixel intensity. The limited distribution function lowers the image

contrast of brightness pixels while increasing the contrast of low contrast pixels.

3.5. Edge Detection

A group of connected pixels situated between the edges of two regions in an image is referred to as an edge. Edges in binary images are black pixels that have one white neighbour. Sobel edge detection is the technique for identifying and extracting edges from digital images in order to get critical image analysis details. The result of the leukaemia and red blood cell edge detection technique are provided. There is a substantial variation in the size, shape, quantity, and location of leukaemia cells and red blood cells. The edge detection images are depicted in fig.3

3.6. Feature extraction

The feature extraction is a crucial stage that utilized for removing the irrelevant features present in the input images to diagnose leukemia. The pre-tuned models such as ResNet-50 and VGG-19 was trained on ImageNet, which contains a variety of image classifications
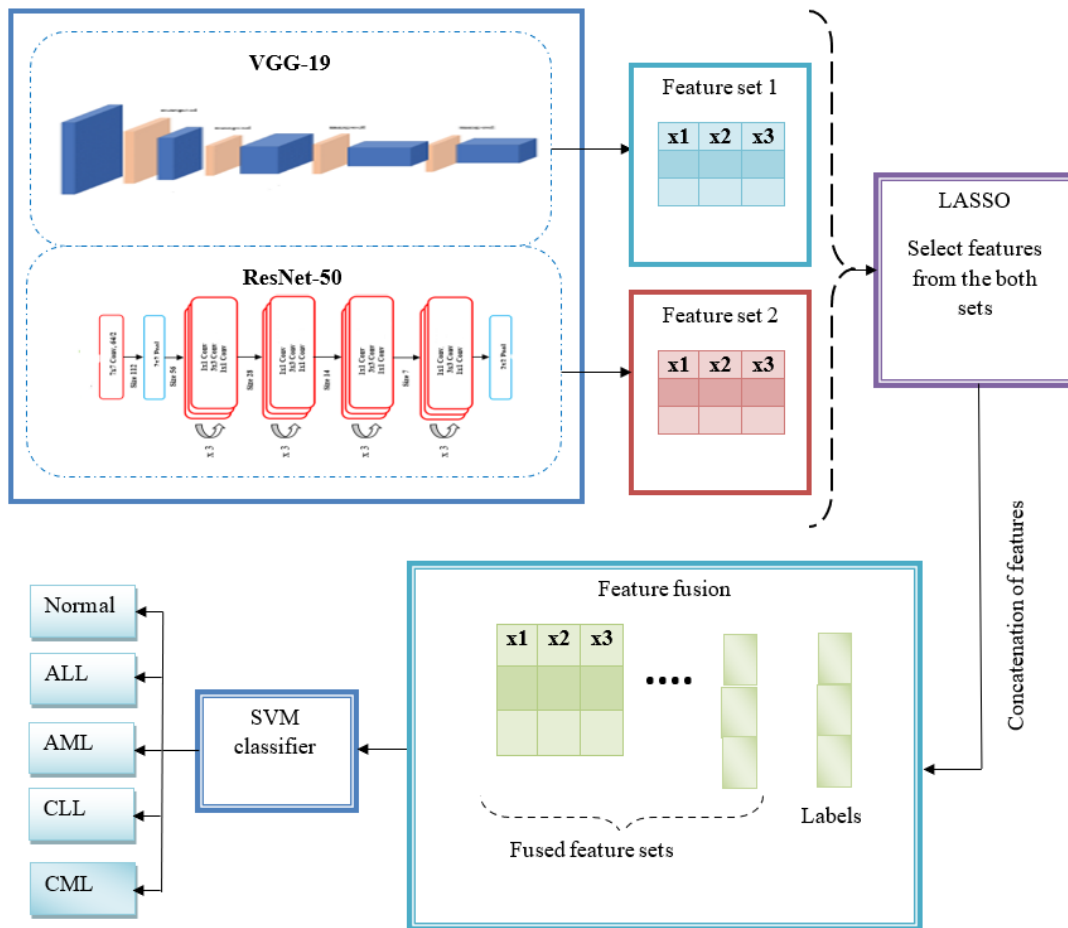

Figure 4. Architecture of the proposed transfer learning model

These models are trained on various set of images divided into various set of categories. Because the model was tuned on such a large dataset, it has built a better representation of minimal level characteristics including spatially, boundaries, rotational, brightness, and structures that can be used across dissimilar computer vision issues to allow information flow and operate as a feature extractor for the input images.

VGG-19 is used to analyse the effect of the convolutional neural networks depth by extracting the structural features. Using a 3x3 convolution filter size and 11x11 convolutional filter size, this model acquires one of the best results in the ILSVRC 2014, with improved feature extraction. Small filters improve the network's depth rather than its width in this architecture, which is crucial for achieving greater performance. Initially, the model was trained on the datasets to retrieve deep features using the transfer learning approach. This model is loaded by the dataset paths for randomly selects the input images, 70% for tuning, and 30% for testing. The function of cross-entropy is used to activate the average pooling layers and FC layers of the system. The extracted features are considered as feature set 1.

ResNet-50 is based on the principle of generating deep CNN than existing simpler networks while also establishing out the numerous layers to eliminate the over-fitting issue. Using the transfer learning approach, the model was initially trained on the datasets to extract deep features. In this model the dataset paths are loaded for arbitrary takes the input images, 70% for training, and 30% for testing. The cross-entropy function is used to activate the average pooling

layers and FC layers of the architecture and the extracted features are considered as feature set 2.

3.7. Feature selection

The feature selection reduces the dimensions of the image by selecting a set of features by using LASSO. It is commonly known technique; here it performs feature selection and regression simultaneously while imposing standard constraints l_1 on the coefficients of regression. The non-differentiability of the normativel_1, on either, prevents from evaluating the objective of gradient function. Then LASSO algorithm learns sparse regression coefficients as,

$$\beta_0 = argmin_\beta \ ||x - Y\beta||^2 + \alpha||\beta|| \ l_1 \qquad (6)$$

Where response vector $= x_1, x_2 \ldots \ldots x_n$, the feature matrix $y = y_1, y_2 \ldots \ldots y_n$ and α is a trade-off parameter in determining comparative fitting efficiency and sparsity of β_0.

3.8. Feature fusion

In the field of disease recognition, the feature concatenation is an important step. To create a finished mono feature vector for illness diagnosis, the individual feature vectors are gradually fused. The key justification for carrying out this phase is to combine all descriptor data into a single feature vectors column, which can be useful in lowering the error rates. By removing the unnecessary characteristics from the input image as feature sets 1 and 2, the VGG-19 and ResNet-50 extract the structural and geometric features. The relevant or specific features are subsequently selected from the retrieved features using the fusion selection approach, and these features are combined to classify leukemia.

3.9. Classification

SVM locates and uses a hyperplane class border that maximizes the space in the training dataset to identify binary classes. The training data samples that follow the class boundary hyperplanes form the support vectors, and the margins are the spaces between the support vectors and the class border hyperplanes. It is based on the notion of decision planes, which set decision boundaries. A decision plane makes a distinction between the features of images that belong to several classes.

The training and testing data for this classification procedure frequently contains a variety of data examples. The training set has several features and class labels for each instance. The dynamically dividing hyperplane with the greatest margin and filter count is then found by the SVM. Using the gathered support vectors, the kernel is changed in a data-dependent manner to obtain the outcomes. Depending on these findings, it may be determined whether the patient have leukemia or healthy.

4. RESULTS AND DISCUSSIONS

The proposed method consists of two networks such as ResNet-50 and VGG-19 for predicting and classifying the types of leukemia with high accuracy and minimal computational cost. These networks perform on the basis of transfer learning, since the performance analysis and comparative analysis was discussed in this section.

4.1. Performance analysis

In this study the performance assessment is considered on the basis of specificity, accuracy, precision, recall and F1 score.

$$s = \frac{Tp}{Tn + Fp} \qquad (7)$$

$$r = \frac{Tp}{Tp + Fn} \qquad (8)$$

$$p = \frac{Tp}{Tp + Fp} \qquad (9)$$

$$a = \frac{Tp + Tn}{Total \ no.of \ samples} \qquad (10)$$

$$F1 = \frac{2*p*r}{p+r} \qquad (11)$$

The performance analysis is shown below table 4.3based on the datasets namely ALL-IDB for ALL and normal and Ash dataset for CLL, CML and AML

Table 1. Performance analysis of the proposed model

Datasets	Classes	Specificity	Precision	Recall	F1 score	Accuracy
ALL-IDB	Normal	99.2	99.4	99.5	98.3	99.8
	ALL	99.8	98.5	97.1	98.6	99.5
ASH dataset	AML	97.5	95.3	95.0	94.2	97.0
	CLL	95.3	95.8	94.2	93.1	95.1
	CML	96.4	93.6	92.5	97.5	93.5

From the table1, the proposed model yields the accuracy range for dataset-1 is 99.08% and 99.02% for dataset-2 that is illustrated in fig.5.
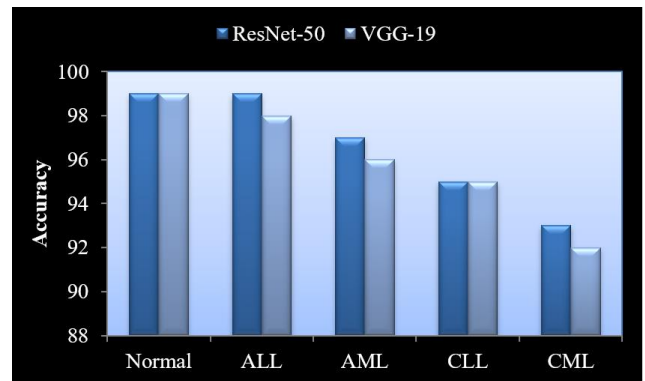

Figure 5. Accuracy acquired by ResNet-50 and VGG-19 based on datsets

From the fig.6 that traditional methods namely Resnet-50 andVGG-16 obtain high accuracy in both dataset by fusing these networks through transfer learning it scores high accuracy rate.
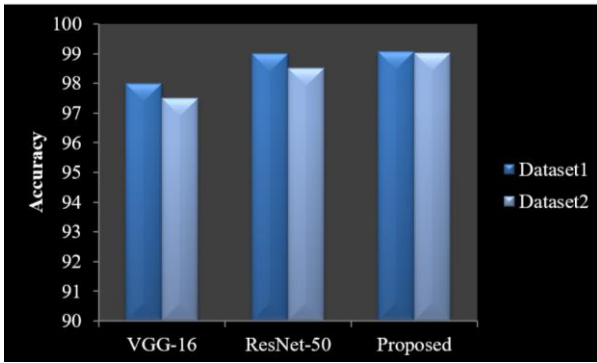
Figure.6. Accuracy acquired by the fusion of proposed method

4.2 Comparative analysis

In this proposed study, the testing methodology is used to detect the leukemia in early stages. The transfer learning with the neural networks such as ResNet-50 and VGG-19 were compared with previous techniques. From that the proposed technique reaches high accuracy than the other deep learning techniques. The accuracy obtained by the proposed model is 99.02%, which is greater than the existing techniques. The comparative analysis is performed between the proposed model and the existing models such as AlexNet+Lenet [1], DCNN [3], CNN+SGD [9] and AlexNet [10] is illustrated in table2,

Table 2. Comparative analysis of five existing models

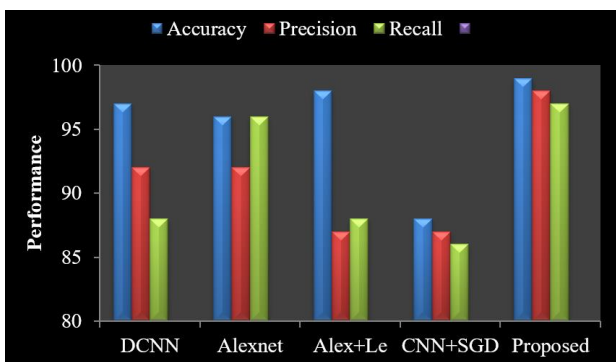| Networks	Accuracy	Precision	Recall	Specificity	F1 score
DCNN [3]	97.02	92.4	8.3	87.5	89.1
AlexNet [10]	96.06	92.1	96.74	99.3	98.2
AlexNet+Lenet [1]	98.58	87.4	88.5	92.7	91.5
CNN+SGD [9]	88.74	87.3	86.4	85.6	87.3
Proposed method TL+SVM	99.08	98.5	97.1	99.5	97.5

Figure 7. Graphical comparison between five deep neural networks

The outcomes of each network were compared to establish that the suggested method's result is more efficient. The range of accuracy obtained by the proposed network is 99.08% and 99.02% for both datasets. The computational cost drastically reduced compared to other networks. Then, comparison is made between the machine learning classifiers namely Random Forest (RF), Decision tree (DT), Naive Bayes (NB), k-nearest neighbour (kNN), and Support vector machine (SVM). The table.3 depicts the comparison between the machine learning classifiers and the graphical comparison is shown in figure 7. From this analysis SVM is outperformed than the other classifiers while preserving the accuracy.

Table 3. Comparison of different machine learning classifiers

Models	Accuracy	Precision	Recall	Specificity	F1 score
RF	96.5	95.7	92.0	90.0	91.2
DT	92.1	98.2	93.2	91.0	94.7
NB	93.4	94.2	94.1	90.5	94.2
KNN	92.4	93.7	88.0	86.0	87.2
SVM	99.2	94.9	94.0	95.1	98.6

From the table 3, the existing machine learning classifiers perform much slower than the SVM. Since the proposed methodology has the fusing the deep learning networks with SVM classifier to classify the types of leukaemia and it acquire high classification accuracy.
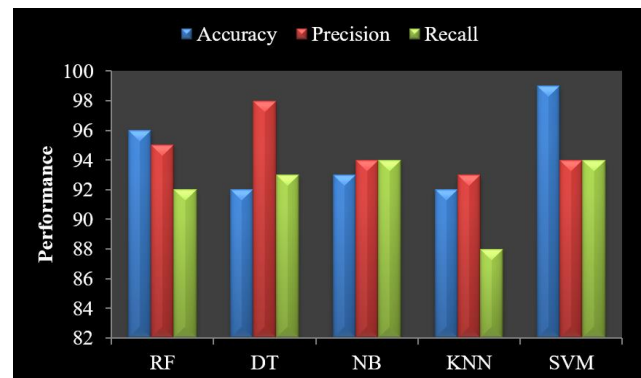
Figure 8. Graphical comparison of different ML classifiers

From the above comparisons, it is obvious that the proposed model gains better accuracy range of 99.08% and 99.02% at slight computational cost. This classification and recognition are very essential for initiation of immediate and effective therapy to the affected individuals by leukemia. However, there are some limitations by using Sobel edge detector, the gradient magnitude of the edges reduces as noise rises, subsequent in erroneous fallouts. In future the accuracy is improved by using the better and advance edge detection technique.

5. CONCLUSION

Transfer learning is a method that is currently being developed for image processing, and it is useful for resolving issues with early-stage leukemia analysis. At this firm, the proposed method uses transfer learning for extracting the features and classifies the four major types such as ALL, AML, CLL, CML and normal. The result shows that the proposed model can extract the structural features for early prediction by recognizing the changes in the blood cells. In the above results, conclude that the proposed model gains high accuracy on both training and testing datasets compared to other deep neural network. The proposed method outperforms with drastically minimum computational cost while preserving the accuracy rate of 99.08% and 99.02%. By using this method, the rate of detection can be raised and the affected patients can receive immediate and suitable clinical care. In the future, this technology may be used in hospitals to further the advancement of AI in the medical industry and to more effectively improve leukemia detection.

CONFLICT OF INTEREST

The author proclaims that there are no conflicting interests to disclose in this study.

REFERENCES

[1] M. Shaheen, R. Khan, R.R. Biswal, M. Ullah, A. Khan, M.I. Uddin, M. Zareei, and A. Waheed, "Acute Myeloid Leukemia (AML) Detection Using AlexNet Model", *Complexity*, 2021. [CrossRef] [Google Scholar] [Publisher Link]

[2] P.K. Das, P. Jadoun, and S. Meher, "Detection and classification of acute lymphocytic leukemia". In 2020 IEEE-HYDCON, pp. 1-5. 2020, September. IEEE. [CrossRef] [Google Scholar] [Publisher Link]

[3] D. Kumar, N. Jain, A. Khurana, S. Mittal, S.C. Satapathy, R. Senkerik, and J.D. Hemanth, "Automatic detection of white blood cancer from bone marrow microscopic images using convolutional neural networks", *IEEE Access*, vol. 8, pp.142521-142531, 2020. [CrossRef] [Google Scholar] [Publisher Link]

[4] S. Tammina. "Transfer learning using vgg-16 with deep convolutional neural network for classifying images". *International Journal of Scientific and Research Publications (IJSRP)*, vol. 9, no.10, pp.143-150, 2019. [CrossRef] [Google Scholar] [Publisher Link]

[5] G. Cao, L. Huang, H. Tian, X. Huang, Y. Wang, and R. Zhi, "Contrast enhancement of brightness-distorted images by improved adaptive gamma correction", *Computers & Electrical Engineering*, vol. 66, pp.569-582, 2018. [CrossRef] [Google Scholar] [Publisher Link]

[6] S. Rahman, M.M. Rahman, M. Abdullah-Al-Wadud, G.D. Al-Quaderi, and M. Shoyaib. 2016. "An adaptive gamma correction for image enhancement", *EURASIP Journal on Image and Video Processing*, vol. 2016, no.1, pp.1-13. [CrossRef] [Google Scholar] [Publisher Link]

[7] M. Veluchamy, and B. Subramani. "Image contrast and color enhancement using adaptive gamma correction and histogram equalization". *Optik*, vol. 183, pp.329-337, 2019. [CrossRef] [Google Scholar] [Publisher Link]

[8] M. Loey, M. Naman, and H. Zayed. "Deep transfer learning in diagnosing leukemia in blood cells", *Computers*, vol. 9, no.2, p.29, 2020. [CrossRef] [Google Scholar] [Publisher Link]

[9] N. Ahmed, A. Yigit, Z. Isik, and A. Alpkocak, 2019. "Identification of leukemia subtypes from microscopic images using convolutional neural network". *Diagnostics*, vol. 9, no.3, p.104. [CrossRef] [Google Scholar] [Publisher Link]

[10] S. Shafique, and S. Tehsin, "Acute lymphoblastic leukemia detection and classification of its subtypes using pre trained deep convolutional neural networks", *Technology in cancer research & treatment*, vol. 17, p.1533033818802789, 2018. [CrossRef] [Google Scholar] [Publisher Link]

[11] A. Rehman, N. Abbas, T. Saba, S.I.U. Rahman, Z. Mehmood, and H. Kolivand, "Classification of acute lymphoblastic leukemia using deep learning". *Microscopy Research and Technique*, vol. 81, no.11, pp.1310-1317, 2018. [CrossRef] [Google Scholar] [Publisher Link]

[12] S.H. Kassani, P.H. Kassani, M.J. Wesolowski, K.A. Schneider, and R. Deters, 2019, October. "A hybrid deep learning architecture for leukemic B-lymphoblast classification", In 2019 International Conference on Information and Communication Technology Convergence (ICTC), pp. 271-276. IEEE. [CrossRef] [Google Scholar] [Publisher Link]

[13] S. Saleem, J. Amin, M. Sharif, M.A. Anjum, M. Iqbal, and S.H. Wang, 2021. "A deep network designed for segmentation and classification of leukemia using fusion of the transfer learning models", *Complex & Intelligent Systems*, pp.1-16. [CrossRef] [Google Scholar] [Publisher Link]

[14] M. Ghaderzadeh, F. Asadi, A. Hosseini, D. Bashash, H. Abolghasemi, and A. Roshanpour, 2021. "Machine learning in detection and classification of leukemia using smear blood images: a systematic review", *Scientific Programming*, 2021. [CrossRef] [Google Scholar] [Publisher Link]

[15] A. Abhishek, R.K. Jha, R. Sinha, and K. Jha, 2022. "Automated classification of acute leukemia on a heterogeneous dataset using machine learning and deep learning techniques", *Biomedical Signal Processing and Control*, vol. 72, p.103341. [CrossRef] [Google Scholar] [Publisher Link]

[16] I.J. Maria, T. Devi, and D. Ravi, 2020. "Machine learning algorithms for diagnosis of leukemia". IJSTR, vol. 9, pp.267-270. [CrossRef] [Google Scholar] [Publisher Link]

[17] F.M. Talaat, and S.A. Gamel, Machine learning in detection and classification of leukemia using C-NMC_Leukemia. *Multimedia Tools and Applications*, pp.1-14, 2023. [CrossRef] [Google Scholar] [Publisher Link]

[18] T.T.P. Thanh, C. Vununu, S. Atoev, S.H. Lee, and K.R. Kwon, 2018. "Leukemia blood cell image classification using convolutional neural network". *International Journal of Computer Theory and Engineering*, vol. 10, no.2, pp.54-58. [CrossRef] [Google Scholar] [Publisher Link]

[19] Y. Liu, and F. Long, "Acute lymphoblastic leukemia cells image analysis with deep bagging ensemble learning. In ISBI 2019 C-NMC Challenge: Classification in Cancer Cell Imaging", pp. 113-121, 2019. [CrossRef] [Google Scholar] [Publisher Link]

[20] H.T. Salah, I.N. Muhsen, M.E. Salama, T. Owaidah, and S.K. Hashmi, "Machine learning applications in the diagnosis of leukemia: Current trends and future directions". *International journal of laboratory hematology*, vol. 41, no.6, pp.717-725, 2019. [CrossRef] [Google Scholar] [Publisher Link]

[21] K.A.A. Daqqa, A.Y. Maghari, and W.F. Al Sarraj, "Prediction and diagnosis of leukemia using classification algorithms". In 2017 8th International Conference on Information Technology

(ICIT), pp. 638-643, 2017. IEEE. [CrossRef] [Google Scholar] [Publisher Link]

[22] K.A. Karunharan, and O. Prakash. "Automatic preprocessing of blood cells using edge detectors for the detection of leukemia". *International Journal of Pharmaceutical Research*, vol. 11, no.1, 2019. [CrossRef] [Google Scholar] [Publisher Link]

[23] L.G. Falconí, M. Pérez, and W.G. Aguilar, "Transfer learning in breast mammogram abnormalities classification with mobilenet and nasnet. In 2019 International Conference on Systems", *Signals and Image Processing (IWSSIP)*, IEEE, pp. 109-114, 2019. [CrossRef] [Google Scholar] [Publisher Link]

[24] R. Kaur, and R. Maini, "Evaluation and Analysis of Edge Detection Techniques on Leukemia Images". [CrossRef] [Google Scholar] [Publisher Link]

[25] Ahmad, R., Awais, M., Kausar, N., Tariq, U., Cha, J.H. and Balili, J., 2023. Leukocytes Classification for Leukemia Detection Using Quantum Inspired Deep Feature Selection. *Cancers*, 15(9), p.2507. [CrossRef] [Google Scholar] [Publisher Link]

[26] S. Ansari, A.H. Navin, A.B. Sangar, J.V. Gharamaleki, and S. Danishvar, A customized efficient deep learning model for the diagnosis of acute leukemia cells based on lymphocyte and monocyte images. *Electronics*, vol. 12, no.2, p.322, 2023. [CrossRef] [Google Scholar] [Publisher Link]

[27] M.A. Sarder, M. Maniruzzaman, and B. Ahammed, "Feature Selection and Classification of Leukemia Cancer Using Machine Learning Techniques". *Machine Learning Research*, vol. 5, no. 2, p.18, 2020. [CrossRef] [Google Scholar] [Publisher Link]

[28] M.S. Yang, and W. Ali, "Fuzzy Gaussian Lasso clustering with application to cancer data", *Mathematical Biosciences and Engineering*, vol. 17, no.1, pp.250-265, 2020. [CrossRef] [Google Scholar] [Publisher Link]

[29] L.H. Vogado, R.M. Veras, F.H. Araujo, R.R. Silva, and K.R. Aires. "Leukemia diagnosis in blood slides using transfer learning in CNNs and SVM for classification", *Engineering Applications of Artificial Intelligence*, vol. 72, pp.415-422, 2018. [CrossRef] [Google Scholar] [Publisher Link]

[30] A. Genovese, M.S. Hosseini, V. Piuri, K.N. Plataniotis, and F. Scotti. "Histopathological transfer learning for Acute Lymphoblastic Leukemia detection", In 2021 IEEE International Conference on Computational Intelligence and Virtual Environments for Measurement Systems and Applications (CIVEMSA), pp. 1-6. IEEE, 2021. [CrossRef] [Google Scholar] [Publisher Link]

[31] P. Manescu, P. Narayanan, C. Bendkowski, M. Elmi, R. Claveau, V. Pawar, B.J. Brown, M. Shaw, A. Rao, and D. Fernandez-Reyes, Detection of acute promyelocytic leukemia in peripheral blood and bone marrow with annotation-free deep learning. *Scientific Reports*, vol. 13, no. 1, p.2562, 2023. [CrossRef] [Google Scholar] [Publisher Link]

[32] W. Wang, X. Yuan, Z. Chen, X. Wu, and Z. Gao, "Weak-Light Image Enhancement Method Based on Adaptive Local Gamma Transform and Color Compensation". *Journal of Sensors,* 2021. [CrossRef] [Google Scholar] [Publisher Link]

AUTHORS

P. G. Sreelekshmi currently working in University Institute of Technology Malayinkeezhu under University of Kerala as Lecturer. Prior to her recent appointment she was worked at Sivaji College of Engineering as Assistant Professor. She completed her ME in 2014 from Anna University Chennai.

P. Linu Babu is Currently working as an Assistant Professor in IES College of Engineering Thrissur, Kerala. Her Interested research area is Digital Image Processing. Her Teaching Experience is 11 Years.

P. Josephin Shermila, She was born in Kanyakumari District, Tamilnadu, India in 1983. She received her B.E. degree in Electronics and Communication Engineering from Noorul Islam college of Engineering, Kumaracoil, Anna University, India in 2005, and obtained M.E. degree in Computer Communication Engineering from National Engineering College, Kovilpatti, Anna University, India in 2007. She has completed her research in Information and Communication Engineering in Anna University, Chennai, India in 2021. She worked as a Programmer Analyst in Cognizant Technology Solutions from October 2007 to October 2010. She is in teaching profession since November 2010. Currently she is working as Associate Professor in the Department of Artificial Intelligence and Data Science, RMK College of Engineering and Technology, Thiruvallur District- 601206, India. She is a member of few professional bodies and have given few guest lectures in reputed organizations She has published more than 19 articles and has published 15 conference papers. Her research area of interest is Nutrition Estimation from Food Images, Image Processing, Machine Learning and Deep Learning.

RESEARCH ARTICLE

ALZHEIMER DISEASE DETECTION VIA DEEP LEARNING BASED SHUFFLE NETWORK

D. S. Dakshina[1, *], Della Reasa Valiaveetil[2] and A. Bindhu[3]

[1]Lecturer in Computer science, Department of BCA, UIT vellarada, Aarattukuzhi, Vellarada, Kerala, India.
[2]Assistant Professor, Department Electrical Communication Engineering, Christ College of Engineering, Irinjalakuda, Thrissur, Kerala, India.
[3]Research Scholar, Department of Computer Science and Research, S.T. Hindu College, Nagercoil, India.

*Corresponding e-mail:dakshinadayandan@gmail.com

Abstract – Alzheimer's disease (AD) is a progressive neuro de-generative ailment that decimates the brain memory. The early stage of Alzheimer's is mild cognitive impairment (MCI) and it is hardly possible to diagnosis. Artificial intelligence (AI) has proliferated in recent years across all scientific disciplines. The early detection of AD is now more accurate and precise thanks to the application of AI in medicine. In the proposed study, introducing a novel technique named ShuffleNet for prognosticating dementia, which is intended to assist doctors in diagnosing AD. Magnetic resonance imaging (MRI) was collected from Alzheimer's disease Neuroimaging Initiative-3 (ADNI-3) and pre-processed using Histogram Equalization (HE). ShuffleNet a deep neural network combined with the leaky ReLU was used for extracting the surface features from brain MRI. Finally, the proposed system's effectiveness was demonstrated by the correct classification that was acquired using the multi-layered perceptron (MLP) classifier. When compared to CNN's current networks, the suggested model's findings are the best and most accurate. This model yields the sensitivity range of 98.22%, specificity range of 98.75% and accuracy rate of 99.72% respectively with the minimal computational cost.

Keywords – Alzheimer Disease, Artificial Intelligence, ShuffleNet, Learning, Brain Magnetic Resonance Images

1. INTRODUCTION

A common brain condition that primarily affects elderly persons is Alzheimer's disease (AD). After heart disease, cancer, and brain hemorrhage, it ranks as the fourth most common cause of death around the world [1]. Each year, a reported 10 million infection cases occur. From a neurological standpoint, AD is a chronic neurodegenerative condition that damages brain tissue and induces neuronal cell death. As a result, the patient slowly loses cognitive function and memory, a condition called senile dementia.

Dementia affects over 50 million people globally, 60% of whom living in low- and middle-income nations. 5-8% of people over 60 in the general society currently have dementia [1]. By 2030, 82 million people will have dementia, and by 2050, 152 million people will have dementia, according to projections. The majority of this growth may be traced to the rise in dementia prevalence in developing and middle-income countries.

Additionally, Alzheimer's disease impairs a patient's capacity to talk, write, and read on a daily basis as well as their ability to recognise friends and family. He advances through the early, intermediate cognitive, and late phases of Alzheimer's disease (AD). People in the medium cognitive stage respond fiercely, but patients in the late stage have heart failure and severe respiratory dysfunction [2].
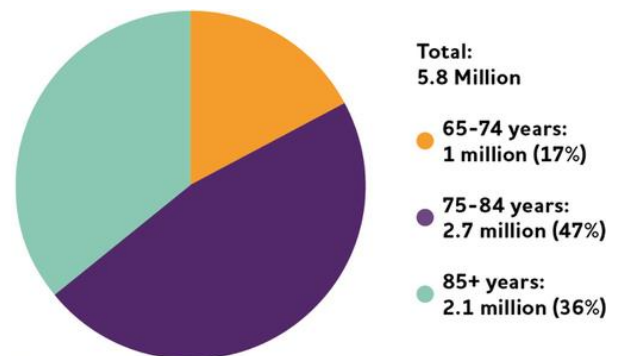
Figure 1. Different age of peoples with Alzheimer's Dementia

Estimates show that 5.8 million Americans 65 and older suffer from dementia connected to Alzheimer's. 80 percent of people are above 75. One in ten women over the age of 65 who have the condition do so. More people develop Alzheimer's disease as they age. According to Figure 1, Alzheimer's disease affects 3% of persons in the 65–74 age group, 17% of people in the 75–84 age group, and 32% of people in the 85–plus age group. Alzheimer's dementia can affect people younger than 65, although it is far less likely to do so and it is not known how frequently it does.

The shuffle-ADD method has been proposed to predict prognosis in dementia to assist physicians in diagnosing AD. The main contributions of this work are:

- Magnetic resonance imaging (MRI) was acquired by the Alzheimer's Disease Neuroimaging Initiative 3 (ADNI-3) and preprocessed using histogram equalization.
- Combined ShuffleNet deep neural network with his Leaky ReLU to extract surface features from brain MRIs.
- Multilayer Perceptron Classifier (MLP) to prove the efficiency of the proposed system. The rest of this work is organized as follows.

A review of the literature is given in Section II. In Section III, the recommended Shuffle-ADD method is explained. Section IV presents the experimental results, while Section V summarizes the contributions.

2. RELATED WORK

Researchers have recently developed a number of deep learning approaches, mostly to increase the precision with which Alzheimer disease can be identified using brain MRI. There have been numerous studies in the literature attempting to develop automated algorithms to detect morphological and functional lesions in the brain associated with AD using various deep and machine learning methods. Some of those research works are briefly discussed in this section.

In 2023, Balaji, *et al* [3] proposed a hybrid deep learning technique for Alzheimer's disease early detection. They combined MRI and PET with multimodal imaging, convolutional neural networks, and long-term short-term memory methods. The proposed model's accuracy improved to 98.5%.

In 2023, Marwa, *et al* [4] develop a deep learning-based pipeline for precise AD stage classification and diagnosis. They employed 2D T1-weighted magnetic resonance imaging (MR) brain pictures and convolutional neural network (CNN) architecture. The next step is to divide MCI into three groups: very mild dementia (VMD), mild dementia (MD), and moderate dementia (MoD). stage before AD. The accuracy rate of the suggested model is 99.68%.

In 2021, Murugan, *et al* [5] proposed the accuracy of AD classification is considerably increased by using the CNN approach to extract features. In order to precisely and visually display each individual's risk of AD, the proposed model builds high resolution (HR) disease probability maps from regional brain regions to multi-layered perceptrons. The proposed model is 97% accurate.

In 2022, Ghazal, T.M, *et al* [6] Brain MRI was used to classify the pictures into four stages: mild dementia (MD), moderate dementia (MOD), non-dementia (ND), and very mild dementia (VMD). The suggested transfer learning on multi-class categorization using brain MRI. The accuracy of the suggested system model is 91.70%.

In 2022, Nguyen, D,*et al* [7] proposed an approach to ensemble learning that blends machine learning and deep learning. The Alzheimer's Disease Neuroimaging Initiative (ADNI) dataset of brain MRI images was used to train and evaluate the method [8-10]. The proposed system model has an accuracy of 96.2% [11-15].

3. PORPOSED MODELLING

In this paper Magnetic resonance imaging (MRI) is collect from Alzheimer's Disease Neuroimaging Initiative-3 (ADNI-3) and it is pre-process using histogram equalization. The output is sent to the ShuffleNet deep neural network combined with the leaky ReLU. It is use for extracting the surface features from brain MRI and the multi-layered perceptron (MLP) classifier, which proves the efficiency of the Shuffle-ADD.

3.1. Preprocessing

The Magnetic resonance image (MRI) is sent to the preprocessing unit. Preprocessing is a great way to enhance the quality of photographs and prepare them for analysis and additional processing. Noise reduction, contrast improvement, image scaling, color correction, segmentation, feature extraction, and other effective image preparation methods are available.

3.1.1. Data Augmentation

The data augmentation component receives a magnetic resonance image (MRI) as input and process it. A technique called data augmentation makes new learning data out of old learning data. Picture data augmentation, which comprises creating modified versions of training data set pictures that belong to the same class as the original image, is perhaps the most well-known type of data augmentation.

Techniques for image modification used in transformation include shift, mirroring, and zooming.

Random picture flips, crops, rotations, stretches, and zooms are examples of geometric image transformations. Additionally, brightness, contrast, and RGB color channels are all modified at random by colorspace conversion. Kernel filters sporadically alter an image's sharpness or blurriness. Particular parts of the original image are randomly deleted. Multiple photos are blended when you merge them.

3.1.2. Histogram Equalization

The histogram equalization process equalizes the digitalized input image (MRI). A contrast enhancing method that works well on practically any kind of image is histogram equalization. By altering the intensity histogram, contemporary techniques like histogram equalisation alter the dynamic range and contrast of a picture.

The Histogram Modelling operator, in contrast to the Contrast Stretch operator, transforms the pixel intensity values in the input and output images using non-linear and non-monotonic transfer functions.

An optimized histogram.

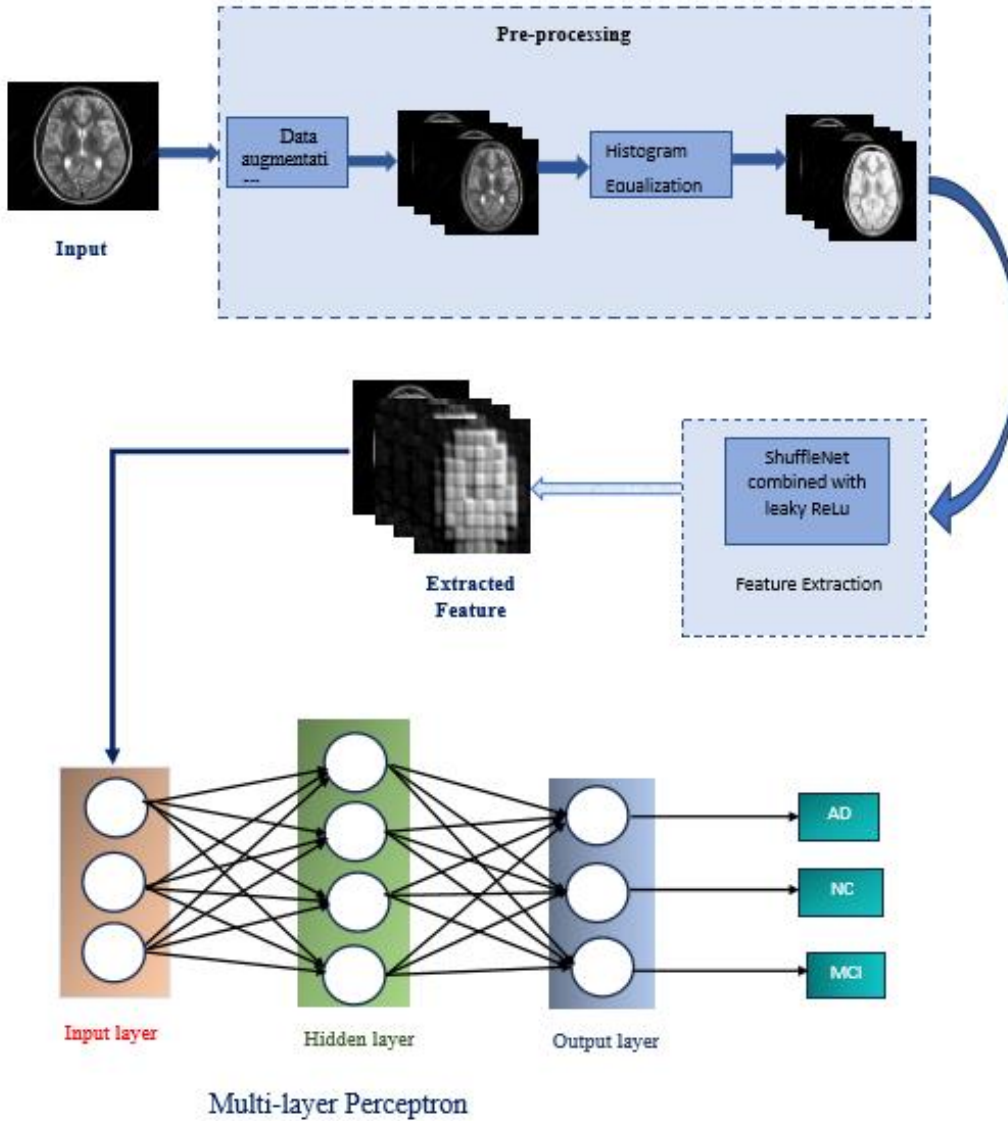P(n) = total number of pixels / number of pixels with strength

Figure 2. Proposed method working architecture

3.2. ShuffleNet

Shuffle-ADD was employed in the suggested study to attain improved accuracy with less processing. Use the Shuffle-ADD model in accordance with your hardware resources for computing. Figure 3 depicts the framework's architecture. The suggested model has 50 learnable layers, making it more complex than a typical CNN. With this architecture, accuracy is maintained while computational costs are minimized thanks to pointwise group convolution and channel shuffling. A 1x1 kernel, or a kernel that iterates over each point, is the kernel used in a pointwise convolution. This kernel's depth reflects how many channels the input image has. Depthwise separable folds are an effective type of folds that may be made by combining this with depth folding.

In Shuffle-ADD, magnetic resonance image preprocessing is carried out with 10-150 MFLOPs of processing power, Shuffle-ADD is thought to be a very computationally efficient CNN architecture created for mobile devices. A convolutional neural network designed for mobile devices with very limited processing power, Shuffle-ADD uses point-wise group convolution and channel shuffle to lower compute expenses while maintaining accuracy.

Our model accepts a 224×224 input image (magnetic resonance image) for processing as its first layer's input. The convolutional layer uses 24 kernels (filters) of size 3×3 and step size 2 ×2 to extract features from the 224×224 input picture in order to create the feature map.

The feature map produced by the convolutional layer is calculated as

A (l, m) =(B×C) (l, m) =$\sum_a \sum_b B(b,a)C(l-b, m-a))$

s indicates the feature map output, i indicate image input, then C indicate the kernel of the convolution layer. After the input image has undergone convolutional processes, the size of the output size $o=((l-v)+2t)/(u+1)$ is produced, where l indicate input, t means padding, v indicate kernel size, and u indicate steps.

The output feature map of the first convolutional layer is sent to the ShuffleNet. unit with a shift (stride) of 2X2. The

ShuffleNet unit consists of two 1 1 pointwise group convolutions and three 3X3 depthwise convolutions, totalling three convolutional operations. The BN, ReLU activation function, and channel shuffle operation come after the first pointwise group convolution.
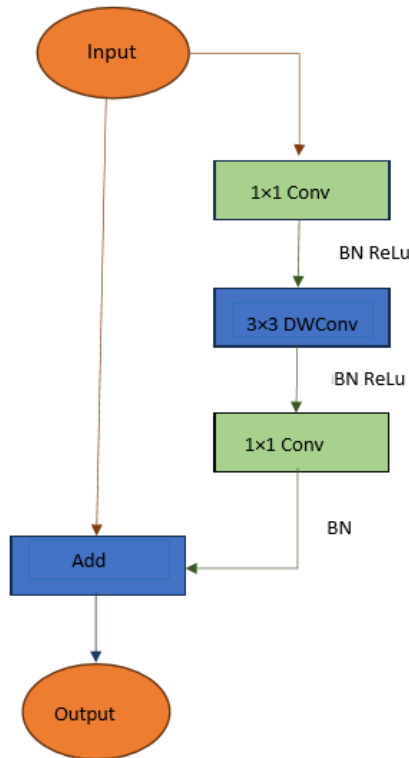

Figure 3. ShuffleNet block diagram

3.3. Multi-layer Perceptron

A multi-layer perceptron (MLP) receives the result of the extracted feature extraction as input. A feedforward neural network extension is MLP. It has three different kinds of layers, as seen in Figure 2: input layer, output layer, and hidden layer. The input layer is where the input signal for processing is received. Utilizing multi-layer perceptrons as classifiers for challenges involving pattern recognition.

The process of extracting a set of characteristics from an object to be classed and using those features to identify the object's class is a typical classification problem. Features in image recognition that are connected to an object's shape include length to width ratio, absolute size, and others. A set of characteristics for a particular item might be thought of as a vector, for example. The feature vector is then analysed to determine the class of each item. A collection of feature vectors with a predetermined categorization are frequently used as the starting point for constructing and testing a classifier. As was already indicated, the ideal features for recognition are not always understood. Additionally, the design set's size must increase as more features are added.

Which features should be employed in the classification problem is strongly related to how multi-layer perceptrons handle wasted input. Less features should be used in general to achieve high classification accuracy. Choosing the ideal

selection of features for categorization is the issue. Different properties are accessible depending on the sensor that was used to display the scene, including: B. Aspect ratio, brightness, edge pixels to total pixels, and contrast ratio.

4. RESULTS AND DISCUSSIONS

In the research paper, the experimental setting was created using MATLAB 2019b. In this examination, the MRI scans from ADNI-3 datasets was used for detecting AD in earlier stages. The efficiency of the proposed Shuffle-ADD model has been evaluated using the specific parameters. Furthermore, the evaluation of the proposed Shuffle-ADD was compared with classic ML models is also provided in this section.

A data set (or dataset) is a group of related pieces of information. When working with tabular data, a data set refers to one or more database tables, with each row denoting a particular record and each column denoting a particular variable. An item's value for each member of the dataset for each variable, such as size and weight, is listed in a dataset. A record can also be a group of papers or files.

4.1. Performance Analysis

In this section, the efficiency valuation was determined using accuracy, f1 score, precision, specificity, and sensitivity (recall). Experimental results of proposed network based on the MRI images shown in Table 1.

Table 1. Experimental results of proposed network based on the MRI images

The specificity is defined as the proportion of recovered true positive samples from the raw samples was gauged. A measurement of the patient & sickness status is the sensitivity

or recall. By classifying the sample MRI images detected as true positives in the patients, it is utilised to assess the accuracy of the outcomes. Some of the parameters are illustrated in equations. where indicates true positives and negatives of the MRI images, and signifies false positives and negatives of the MRI images. The efficiency of the proposed Shuffle-ADD was analysed and it is depicted in Table 2.

Table 2. Performance Analysis of Proposed Shuffle-ADD

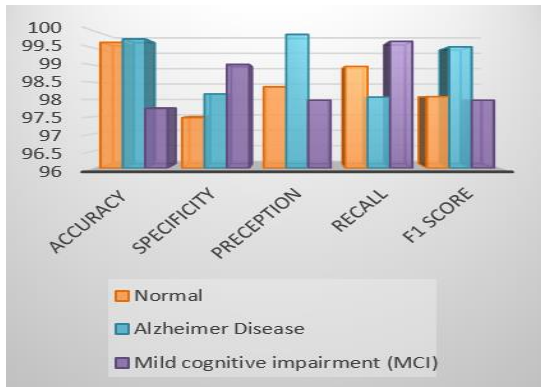| Paramet er	Accu racy	Specifi city	prece ption	Reca ll	F1 Score
Normal	99.66	97.47	98.37	98.96	98.08
Alzheim er Disease	99.76	98.16	99.89	98.07	99.53
Mild cognitive impairme nt (MCI)	97.74	99.02	97.98	99.69	97.98

Figure 4. Performance analysis of proposed Shuffle-ADD based on the system of measurement
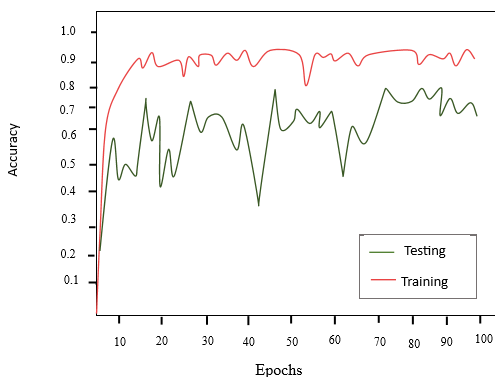

Figure 5. Accuracy curve for proposed Shuffle-ADD

Accuracy curve for proposed Shuffle-ADD SHOWN IN Figure 5. The F1 score, specificity, precision, sensitivity, and accuracy were the key characteristics used to evaluate the effectiveness of the suggested Shuffle-ADD. Table.3 shows the performance evaluation based on the datasets for normal, AD, and MCI. The suggested ShuffleNet successfully classifies NC, AD, and MCI with high accuracy of 99.70%, 99.76%, and 97.70%, respectively. When identifying the

normal class as opposed to the abnormal class, this model achieves good accuracy. Figure 4 shows a visual representation of the suggested Shuffle-ADD's performance analysis. Loss curve for proposed Shuffle-ADD shown in Figure 6.
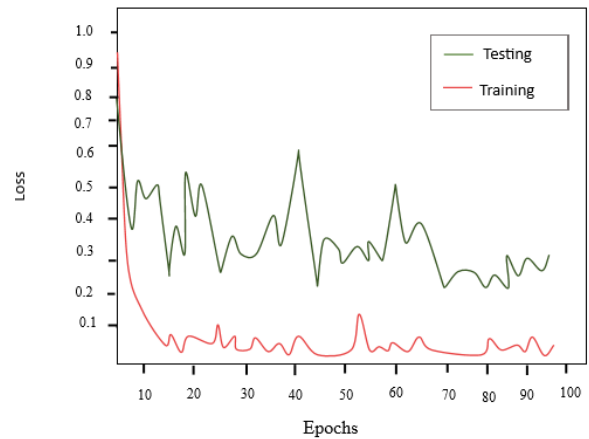
Figure 6. Loss curve for proposed Shuffle-ADD
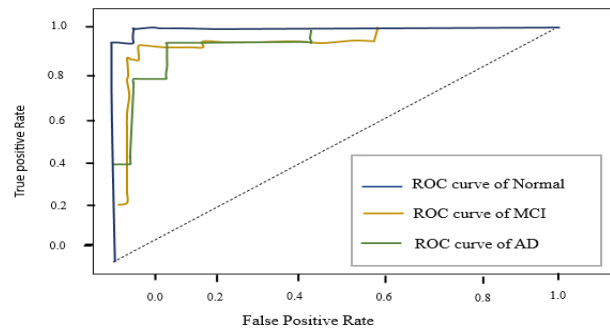
Figure 7. ROC curve of the proposed Shuffle-ADD

Figure 7 shows the Receiver Operating Characteristic (ROC) curve produced for obtained MRI datasets. For the three classes, the suggested Shuffle-ADD achieves a higher Area Under ROC Curve (AUC) of 0.908, which was calculated using True and False positive rate parameters.

4.2. Comparative Analysis

The competence of ML classifiers was estimated for evaluating the fallouts of the proposed Shuffle-ADD obtains better accuracy.
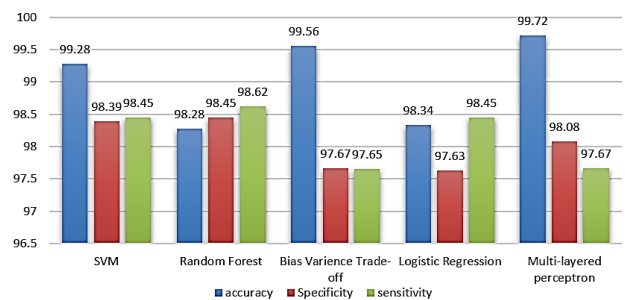
Figure 8. Performance comparison of SVM, Random Forest, Bias Varience Trade-off, Logistic Regression, MLP

The comparative assessment was performed between the proposed Shuffle Net and four ML networks SVM, Random

Forest, Bias Varience Trade-off,Logistic Regression. The performance assessment was carried out using sensitivity, specificity, and accuracy of each ML methods. The accuracy of the proposed Shuffle-ADD is 99.72%, which is greater than the classical ML methods. The performance analysis is shown below figure.8. Accuracy comparison of proposed and state-of-art methods shown in Table 4.

Table 3. Performance comparison of different ML networks

| Parameters	accuracy	Specificity	perception	Recall	F1 Score
SVM	99.28	98.39	98.45	98.08	97.45
Random Forest	98.28	98.45	98.62	98.64	98.08
Bias Varience Trade-off	99.56	97.67	97.65	98.27	98.45
Logistic Regression	98.34	97.63	98.45	97.38	97.07
Multi-layered perceptron	99.72	98.08	97.67	97.79	98.59

Table 4. Accuracy comparison of proposed and state-of-art methods

Authors & year	Methods	Accuracy (%)
Balaji,P, *et al*[3],2023	CNN with LSTM Algorithm	98.5
Marwa,*et al*[4],(2023)	CNN	99.68
Murugan,s,*et al*[4],(2021)	CNN	97
Ghazal, T.M,*et al*[6],(2022)	Transfer Learning Method	91.70
Nguyen, D,*et al*[7],(2022)	Ensemble Learning Method	96.2
Proposed model	Shuffle-ADD	99.72

From this experiment the Multi layered perceptron accuracy is high compared to the other network such as SVM, Random Forest, Bias Varience Trade-off, Logistic Regression, MLP. The acuuracy level is 99.72%. It detects the small variations in the Magnetic Resonance Image (MRI) to diagnosis Alzheimer Disease (AD).

5. CONCLUSION

In this paper, the experimental setting was created using MATLAB 2019b. In this paper Shuffle-ADD, the MRI image from ADNI-3 Alzheimer Disease Neuro-imaging Initiative (ADNI-3) datasets was used for detecting AD in earlier stages. The Multi-Layer Perceptron classify the Alzheimer Disease into normal, mild congnitive impairment and Alzheimer Disease that helps to predict the disease earlier. The proposed Shuffle-ADD obtains the accuracy of 98.08%, 97.25%, and 98.44% for classifying NC, MCI and

AD respectively. The proposed Shuffle-ADD progresses the overall accuracy of 1.67%, 0.04%,8.02% and 3.70% better than CNN with LSTM Algorithm, CNN, Transfer Learning Method, Ensemble Learning Method respectively. In future, the accuracy of the proposed Shuffle-ADD will be progresses in order to precisely detects the grades of AD for improving the accuracy in early diagnosis of Alzheimer disease in its early stages.

CONFLICTS OF INTEREST

The authors declare that they have no known competing financial interests or personal relationships that could have appeared to influence the work reported in this paper.

REFERENCES

1. F. Zhang, "Multi-modal deep learning model for auxiliary diagnosis of alzheimer's disease", Neurocomputing, vol.361, pp. 185-195, 2019. [CrossRef] [Google Scholar] [Publisher Link]
2. A. Mehmood, M, "A deep Siamese convolution neural network for multi-class classification of alzheimer disease", Brain Sci., vol.10, no.2, p. 84, 2020, [CrossRef] [Google Scholar] [Publisher Link]
3. P. Balaji, "Hybridized deep learning approach for detecting Alzheimer's disease", Biomedicines, vol.11, no.1, p.149, 2023. [CrossRef] [Google Scholar] [Publisher Link]
4. E. G. Marwa, "An MRI-based deep learning approach for accurate detection of Alzheimer's disease", Alexandria *Engineering Journal*, vol.63, pp.211-221, 2023. [CrossRef] [Google Scholar] [Publisher Link]
5. S. Murugan, "DEMNET: a deep learning model for early diagnosis of Alzheimer diseases and dementia from MR images". *Ieee Access*, vol. 9, pp.90319-90329, 2021, [CrossRef] [Google Scholar] [Publisher Link]
6. T. M. Ghazal, "Alzheimer Disease Detection Empowered with Transfer Learning", *Computers, Materials & Continua*, vol.70, no.3, 2022. [CrossRef] [Google Scholar] [Publisher Link]
7. D. Nguyen, "Ensemble learning using traditional machine learning and deep neural network for diagnosis of Alzheimer's disease". *IBRO Neuroscience Reports*, vol.13, pp.255-263, 2022. [CrossRef] [Google Scholar] [Publisher Link]
8. A. Shukla, "Review on alzheimer disease detection methods: Automatic pipelines and machine learning techniques". *Sci*, vol.5, no.1, p.13, 2023. [CrossRef] [Google Scholar] [Publisher Link]
9. M. Tanveer, "Machine learning techniques for the diagnosis of Alzheimer's disease: A review". *ACM Transactions on Multimedia Computing, Communications, and Applications (TOMM)*, vol.16, no.1s, pp.1-35, 2020. [CrossRef] [Google Scholar] [Publisher Link]
10. G. Mirzaei, "Machine learning techniques for diagnosis of alzheimer disease, mild cognitive disorder, and other types of dementia". *Biomedical Signal Processing and Control*, vol.72, p.103293, 2022, [CrossRef] [Google Scholar] [Publisher Link]
11. G. Mirzaei, "Imaging and machine learning techniques for diagnosis of Alzheimer's disease". *Reviews in the*

Neurosciences, vol.27, no.8, pp.857-870, 2016. [CrossRef] [Google Scholar] [Publisher Link]

12. J. Song, "An effective multimodal image fusion method using MRI and PET for Alzheimer's disease diagnosis". *Frontiers in digital health*, vol.3, pp.637386, 2021. [CrossRef] [Google Scholar] [Publisher Link]

13. D. Nguyen, "Ensemble learning using traditional machine learning and deep neural network for diagnosis of Alzheimer's disease". *IBRO Neuroscience Reports*, vol.13, pp.255-263, 2022. [CrossRef] [Google Scholar] [Publisher Link]

14. A. G. Howard, "Mobilenets: Efficient convolutional neural networks for mobile vision applications". arXiv preprint arXiv:1704.04861, 2017. [CrossRef] [Google Scholar] [Publisher Link]

15. D. W. Ruck, "Back propagation: A degenerate Kalman filter", IEEE Transactions on Pattern Analysis and Machine Intelligence, June 1989. Submitted for publication. [CrossRef] [Google Scholar] [Publisher Link]

16. R. O. Duda, "Pattern Classification and Scene Analysis". John Wiley and Sons, New York, 1973. [CrossRef] [Google Scholar] [Publisher Link]

17. S. Dudani, K. Breeding, and R. Mcghee, Aircraft identification by moment invariants. IEEE Transactions on Computers C-26, 39–45, 1977, [CrossRef] [Google Scholar] [Publisher Link]

18. D. H. Foley, "Considerations of sample and feature size". IEEE Transactions on Information Theory IT-18, pp.618–626, September 1972. [CrossRef] [Google Scholar] [Publisher Link]

AUTHORS

D. S. Dakshina currently working in University Institute of technology vellarada under university of kerala as lecturer. Prior to her recent appointment she was worked at P A AZIZ college of engineering as asst professor. She completed her ME in 2013 from Anna University with rank.

Della Reasa Valiaveetil Phd Scholar at Veltech Rangarajan Dr. Sagunthala R& D Institute of Science & Technology, Chennai, India. Currently working as Assistant Professor at Christ College of Engineering, Irinjalakuda, Thrissur. She is having 10-year Experience. Interested Research area is Biomedical Image Processing

A. Bindhu is currently working as an Assistant Professor and Head, Department of Computer Science at Infant Jesus College of Arts and Science for Women, Mulagumoodu, Kanyakumari District, Tamil Nadu, India. She has received her B. Sc Degrees in Mathematics from Manonmaniam Sundaranar University, Tirunelveli, India. Master of Computer Applications from Manonmaniam Sundaranar University, Tirunelveli, India. She has awarded Master of Philosophy in Computer Applications from Manonmaniam Sundaranar University, Tirunelveli, India. She is studying Doctor of Philosophy in Computer Applications at Manonmaniam Sundaranar University, Tirunelveli, India under the domain of Digital Image Processing. She is the author of a book cloud computing. She has 10 years of experience in teaching and 10 years of experience in programming She has published papers in Scopus and SCI journals. She is a reviewer of IEEE Access and Computers in Biology and Medicine. Her area of interests is medical imaging, image processing, machine learning and cloud computing

RESEARCH ARTICLE

SECURE STORAGE OF LUNG BRAIN MULTI-MODAL MEDICAL IMAGES USING DNA HOMOMORPHIC ENCRYPTION

S. Gnana Sophia[1]*, K. K. Thanammal[2] and S. S. Sujatha[3]

[1,2,3]Department of Computer Science and Application, St. Hindu College, Nagercoil, 629002, India.

Corresponding e-mail: gnanasophiajournals@gmail.com

Abstract – Protecting the medical data on the online platform for transmitting data is a simple and demanding task. In the modern world, various methods are used to safeguard the digital image such as cryptography, watermarking, and steganography. These methods are used for protecting digital images in order to achieve security objectives such as confidentiality, reliability, and usefulness. In the proposed method, the medical images are encrypted and stored in cloud using DNA Homomorphic Encryption (DNA-HE) algorithm. The key is generated using Rider Optimization Technique to ensure security. It acts as double encryption technique. Homomorphic encryption is an authentication approach that allows one to perform observations on encrypted data by decrypting it. In DNA Homomorphic Encryption algorithm, the input data will be a DNA sequence. The same procedure is used to decrypt the encrypted data. Performance of the proposed technique is evaluated using a number of factors, including execution, encryption, and decryption times.

Keywords: DNA Homomorphic algorithm, Rider Optimization algorithm, Encrypting medical images, Decryption.

1. INTRODUCTION

With advancements in computer analytics and information technology, patient privacy and protection continue to expand as a top priority for healthcare organizations. [1]. One of the most valuable and sensitive forms of data in information systems are medical photographs. In the current trends in cloud computing for patient care, this is a demanding and necessary requirement [3]. The transmission of medical pictures via the internet necessitates the adoption of a strong encryption method that can withstand cryptographic intrusions [2]. Data analysts at most healthcare institutions are sometimes increasingly active in obtaining and examining latest kinds and techniques of under-influenced data, like sensor networks, mobile health, social media, and emails in addition to EHR data [4].

The study of secure communication methods, or cryptography, limits who may read a message's contents to the sender and the intended receiver. When transmitting information virtually, cryptography is used to encrypt and decrypt email and other plain-text messages. Cryptographic procedures are employed to maintain data confidentiality and integrity. Depending on the security criteria and risks involved, several cryptographic systems can be used during data transmission and storage.

As a result of developments in communication, patients' medical record results are now subjected to increased privacy and security risks. Cloud computing is a relatively new concept that will have a significant impact on our lives [1]. Cloud computing is a method of computing that allows cloud users to share resources. Given the large number of individuals and organizations who utilize cloud services, it is critical to guarantee security as well as quick data transfer and sharing. As a result, cloud computing confronts two major difficulties: storage and security [16]. The goal of executing information security efforts is to protect important data and device resources. The protection of data is mainly concerned with safeguarding collected data or shared within cloud applications and computer systems, whereas maintaining an operating system requires securing a computer system's network architecture [1].

The first challenge is developing trust in remote deployment. A cloud is a distributed computing model in which a user's actions are carried out on a remote server in a data center. A client must guarantee that the base framework performs the cloud request on the client's own machine while ensuring consistency and secrecy in a cloud environment. To encode the data and save the encoded data in the cloud, a variety of encryption algorithms were applied. Here we are using DNA Homomorphic Encryption technique to encrypt medical images. Rider optimization algorithm is used for key generation.

Consider developing effective strategies for rigorous knowledge validation and procedure in order to meet the

following goals in terms of ensuring cloud data security and trustworthiness under the previously described demanding design: (1) Storage accuracy: to guarantee that users' data is deposited and preserved in the cloud in a timely and accurate manner. (2) Rapid information error localization: locate the faulty server as rapidly as possible until an information eruption is noticed. (3) Dynamic metadata provision: to maintain a consistent level of cloud data consistency confirmation, even if clients change, add to, or remove documents. Our technique enables an external auditor to review users' outsourced information on the cloud without knowing the specifics of the data stored. The approach used here, unlike current approaches, enables for flexible and efficient public auditing of Cloud Computing.

The remaining portions of this paper are organized as follows. The article gives a quick overview of the relevant work in Section II. The proposed technique is presented in Section III. Section IV's detailed presentation of the experiment's findings shows how effective the proposed strategy is. The last section of the essay is Section V.

2. RELATED WORK

The Homomorphic encryption (HE) technique has been used in several research papers for efficient cloud computing with medical data protection have been discussed below.

In 2020, Elmahdi, E., et al [5] suggested an enhanced AOMDV approach to make data flow in MANETs reliable and safe when hostile nodes are present by distributing the components of the full information into separate channels and utilizing a HE mechanism for cryptographic process. According to the simulation results, the system has a greater throughput and packet distribution ratio which are both desired characteristics for emergency applications on MANETs.

Ullah et al [6] introduced a novel kernel homomorphic encryption technique in 2019. After the number of noises was exceeded, the entire negotiating system failed. The rate of advancement for processing, errors, and noises in the electronic world and cloud computing was accelerating daily. To decrease the growth of sounds and computation, they incorporate a revolutionary kernel HE method. The Ker-HE strategy was utilized to reduce the quantity of sounds by employing kernel and kernel homomorphism. These operations were used to reduce the length of the ciphertext during decryption and to clean up any errors or noise.

In 2017, Zhang et al [7] have presented a general technique based on the HE Scheme for developing a reliable cloud storage system. They were the first to look at the connection between HE schemes and secure cloud storage, and they provide G-SCS, a generic approach to build a Secure Cloud Storage protocol that can be used with any HE Scheme (HES). The proposed G-SCS approach found stable over a concept that meets cloud storage security requirements.

Cheon, J.H., et al [8] presented FHE over integers based on CRT in 2015. This paper discusses the third approach, which is based on the Chinese Remainder Theorem and can be constructed homomorphically. It was discovered that one

particular plaintext/ciphertext combination may defeat this approach. They will address this issue by employing a more effective strategy to introduce an error into a message before encryption. They show that the strategy is completely homomorphic and resistant to chosen-plaintext threats under the approximate GCD presumption and the sparse subset sum assumption, providing a stable update to their original concept.

In 2019, Li, R., et al [9] suggested, FHE-based smart grid anomaly detection system for privacy protection. They presented a LUT method for analyzing any single-integer input variable in this study. At the time, integer encoding was more effective than bitwise encoding. The length of the evaluation was independent of the objective since they employed the LUT approach. This protocol also supported other structures that relied on FHE for a single input challenging function evaluation.

In 2020, Li, et al [10], presented new security concepts. extended IND-CPA protection to incorporate the passive protection requirements for (homomorphic) approximation encryption algorithms. The requirement for suitable authentication notions for approximation encryption illustrates the necessity of concurrently examining correctness and security, two essential characteristics of cryptographic systems.

Velliangiri S., et al [11] proposed an analysis of dimensionality reduction techniques for effective computing in 2019. They look at feature extraction techniques like EMD and PCA, as well as feature filtering techniques like correlation, LDA, and forward selection, to see how efficient and accurate they are. Their ideas were widely employed in DNNs for improving recognition accuracy and diagnosing medical images.

In 2019, Williamson, R. C., et al [12], proposed Dimensionality reduction as a link between extensive neural recordings and extensive network systems. They assist in the development of network models, which will be used to predict future studies. Single-neuron and paired spike train statistics were previously used to connect neuronal data with network models. To depict the multi-dimensional structure of neuronal population functioning, their study has started to integrate neuronal recordings with network models. Working memory, decision-making, muscle coordination, and a number of other topics have all been studied using this method.

In 2016, Wu, Z., et al [13] proposed that Cloud computing will be used to develop a new parallel and distributed paradigm for huge hyperspectral image analysis. They use dimensionality reduction as an example of how cloud computing systems may be used to execute distributed parallel hyperspectral data processing and accelerate hyperspectral data computations.

In 2017, Kim, et al [14] introduced a new HE-based stable KNN query processing method. They also developed an encrypted index method that performs data filtering without revealing data access patterns in order to achieve high query system speed. According to a study, the method

surpasses the present system in terms of query processing costs while preserving user privacy.

In 2016, Wang, Xiaofen [15] proposed a one-round meeting position calculation protocol in which the location service provider interacts with a semi-trusted cloud server that serves as a computing hub and does most of the computations. The computer hub, the meet decision server, and the users all worked together to keep the user location safe from outside and inside threats. In order to examine the protocol's effectiveness, they employ smart phones to assess its mathematical efficiency. The outcomes of the simulation and a comparison of their protocol to one with comparable features show that it is a more efficient and realistic approach.

Different algorithms have been discussed in various papers. In this paper, we present a DNA Homomorphic Encryption for secure storing of medical data to store the medical data in a secure manner.

3. PORPOSED MODELLING

This section describes DNA Homomorphic Encryption technique, where the medical images are saved in the cloud. Here, the medical images are converted to binary form. A DNA strand is created from the binary data. The keys are created using the Rider Optimization Algorithm (ROA) and the DNA sequences are encrypted using homomorphic encryption. After encryption, the encrypted image can be securely stored in cloud. The same process is used for decryption. The block diagram for the DNA Homomorphic encryption method is represented in Fig:1.
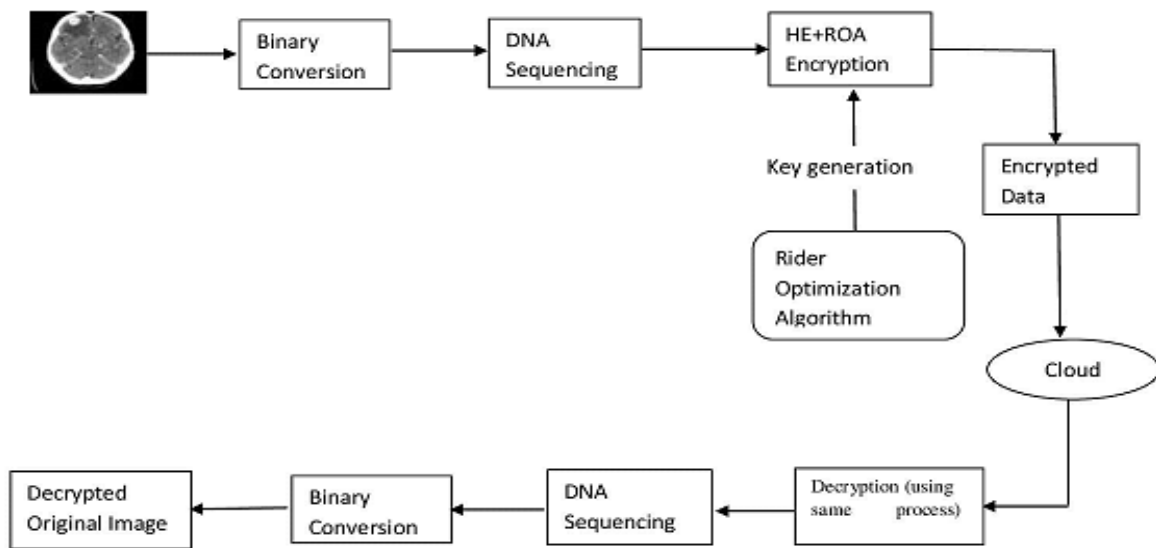

Figure 1. Overall image of the DNA-HE algorithm

3.1 DNA sequencing

Before the image is mapped to a DNA sequence, it must be converted into binary form. Binary digits, often termed as bits, store either 0 or1, attempting to make them the smallest storage units. Adenine(A), guanine(G), cytosine(C), and thymine(T) are the four nitrogenous bases of DNA. Use of the four nucleotides in sequence is the most significant aspect of the DNA-based data masking process. A DNA sequence can be made up of any combination of these nucleotides. When DNA is sequenced, the order of bases can be determined, and they may be represented by single letter in plain sequence format.

Table 1. Binary values for DNA Bases

DNA	BINARY VALUES
A	00
G	01
C	10
T	11

In the above table, the binary values for the DNA bases have been given.

3.2 DNA Homomorphic Encryption

Homomorphic encryption is a form of enciphering technique which permits users to compute on encrypted information without having to decrypt it first. The term "homomorphic" comes from the Greek word "homomorphosis," which means "identical structure". The same mathematical operations on encrypted or decrypted data get the same results because the structure of the data in a homomorphic encryption scheme retains its structure. Homomorphic encryption, unlike other safe computing systems, uses arithmetic functions that focus on addition and multiplication rather than Boolean functions, and only requires a few rounds of interactions. The four operations of this mechanism are key generation, encryption, evaluation, and decryption, which can optionally decrypt the assessment algorithm details. In DNA-HE method the input will be given in the form of DNA sequences.

3.2.1 Key generation

Key generation is the process of creating cryptographic keys. A key is used to encrypt and decode data. A tool or programme that generates keys is known as a keygen. A symmetric key is used to secure both privacy and reliability in a system for encryption keys and authentication and the corresponding image. The primary recognition algorithm has been considering which extra variables can be used to document the public and private keys.

$$Key = ab \ and \ \omega = lcm(u - 1, v - 1) \tag{1}$$

Apply the ROA technique to configure arbitrary encryption and decryption keys for this procedure, then use the optimal private and public key for the remainder of the device's image protection schemes.

3.3 Rider Optimization Algorithm

Riders compete to reach a predetermined destination, which motivates the Rider Optimization Algorithm (ROA). The steps are as follows:

The method is initially started using four groups of riders represented by the letter X, with position initializations done in any order. The group's initiation is determined by

$$M_k = \{M_k(x, y)\} \qquad 1 \le x \le S; 1 \le y \le T \tag{2}$$

Here S represents count of riders and $M_K(x, y)$ represent the position of xth rider in y^{th} size at k^{th} time immediately. The number of riders is calculated by adding the number of cyclists in each group and is represented as,

$$S = R + F + O + K + B \tag{3}$$

Here R represents bypass rider, F represents follower, O represents overtaker, K represents attacker and B represents rag bull rider. $R + F + O + K + B = {S}/{5}$ $\tag{4}$
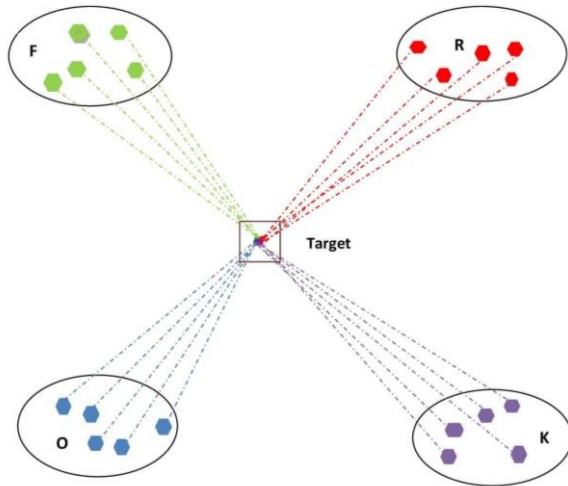

Figure 2. Structure of Rider optimization Algorithm

Following the initialization of rider group settings, each rider's success rate is analyzed. The success rate is computed by multiplying the distance between the rider and the destination by the success rate,

$$Success \ Rate = \frac{1}{\|M_x - k_i\|} \tag{5}$$

Each rider's position in each group is updated in order to establish who is in the lead and who will win. As a result, the rider uses the features of each rider stated in the specification to update the position. The update position of each rider is expressed below

$$M_{k+1}^v(x, j) = M^H(H, j) + \lfloor cos(\varphi_{x,j}^k * M^H(H, j) * \partial_x^k) \rfloor \tag{6}$$

Here j represents coordinate selector, M^H represents leading rider position, H represents leader's index, $\varphi_{x,j}^k$ represents the angle of steering considering x^{th} rider in j^{th} coordinate and ∂_x^k represents the distance.

$$M_{k+1}^j(x, j) = M_k(x, j) + [I_k^*(x) * M^H(H, j)] \tag{7}$$

Here $I_k^*(x)$ denotes direction indicator. The attacker aims to become the leader by following the leader's update procedure, which is defined as follows:

$$M_{k+1}^\alpha(x, \rho) = M^H(H, \rho) + [cos \ \varphi_{x,e}^k * M^H(H, \rho)] + \partial_x^k \tag{8}$$

The standard bypass rider is described as, and the update rule for bypass riders is shown here

$$M_{k+1}^c = \lambda [M_k(Z, T) * \delta(\rho) + M_k(\in, \rho) * [1 - \delta(\rho)] \tag{9}$$

Here λ represents random number, Z represents random number between 1 to T, $\in$ represents random number which ranges between 1 to T and δ represents random number varies between 0 to 1.

Success Rate Calculation

When the updating method is completed, the rate of success for each rider is determined.

Rider Parameter Updating process

To find an appropriate solution, the update parameter for the rider is essential.

Off Time of Rider

For developing an appropriate solution, the parameter of rider's update is crucial.

Algorithm for Rider optimization Algorithm

```
Input: M_K,k, K
Output: M^H
Start
        Initialize solution set
        Initialize other parameters
        Find success rate (5)
While k<K_off
  for x = 1 to T
        Update follower's position (6)
        Update over taker's position (7)
        Update attacker's position (8)
        Update bypass riders' position (9)
        Ranking the riders with rate of success equation (5)
        Select the rider with high rate of success
        Updating the rider parameters
        return M^H
        k = k+1
End for
End While

End
```

The images that are encrypted can be saved in the cloud to complete the encryption process. The data is decrypted using the same procedure that was used to retrieve it. Atlast, the rebuilt image can be received. The decryption process for DNA-HE method is given below.

3.4 Decryption

Data that has been rendered unreadable by encryption can be restored to its original, unencrypted condition through the process of decryption. In the process of decryption, the system gathers and converts the jumbled data into text and graphics that can be understood by both the reader and the system. Both human and automated methods are available for decryption. A combination of keys or passwords can also be used.

$$Decrypted\ image\ = \frac{X(A^{\alpha} mod\ Key_{opt}^2)}{X(X^{\alpha} mod\ key_{opt}^2)}\ mod\ key \quad (10)$$

4. RESULTS AND DISCUSSIONS

This section discussed about the execution of DNA-HE (DNA Homomorphic Encryption Technique). DNA-HE can directly process ciphertext data, effectively ensuring cloud customer data security. DNA-HE is used to encrypt medical data for safe storage. This section explored the consequences of the suggested and current approaches for encrypted photographs.

4.1 Performance analysis

The medical images are saved in cloud in encrypted form in order to provide security. Accessing the medical images for the user is very simple on the other hand unauthorized users cannot be able to access the medical image. The procedure for encryption of medical images is shown in fig:3.
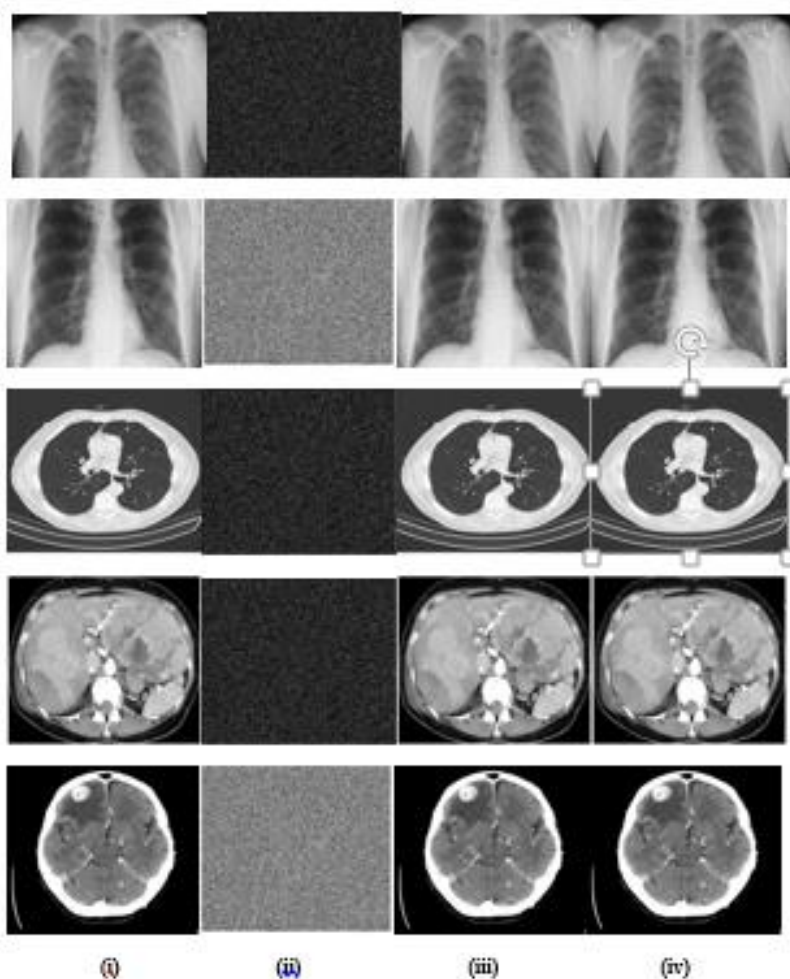

Figure 3. Performance analysis for DNA-HE (i) Original image (ii)Image after encryption (iii)Image after decryption (iv) Rebuilt Original image

The above figure describes the performance analysis of the DNA-HE technique. Encryption is done to securely store the input medical data. The medical images are encrypted and stored in cloud and it can be accessed only by the user. Unauthorized user cannot able to access the images. For decryption, the same method is repeated again and the reconstructed original image will be given. The DNA homomorphic encryption can convert the images to encrypted image is shown above. First the medical images will be converted into binary format and then into DNA sequence, it will be given as input.
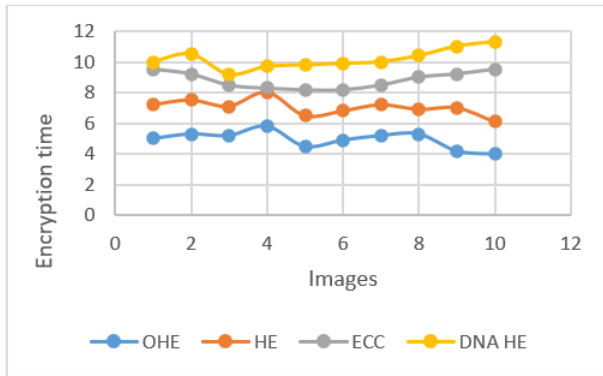
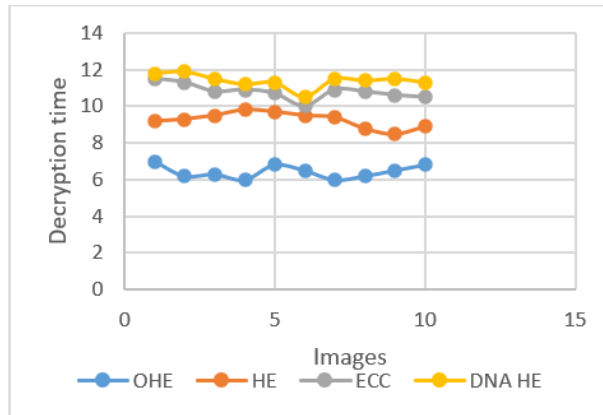**Figure 4.** comparative analysis for encryption time

Figure 5. comparative analysis for decryption time

The figure (4) and (5) depicts a comparison of the proposed method's encryption and decryption times to known methods such as elliptical curve cryptography, homomorphic encryption and optimized homomorphic encryption. Figure 4 shows the encryption time of the recommended approach. Cloud authentication is a means of encrypting or transforming data as it is transported to cloud storage. Cloud Service provider companies encode data and transmit the encryption keys to the user. For decrypting the data, these keys are required. For the encryption time, it is advised that the HE algorithm be reduced by 2% and the ECC algorithm by 4%.
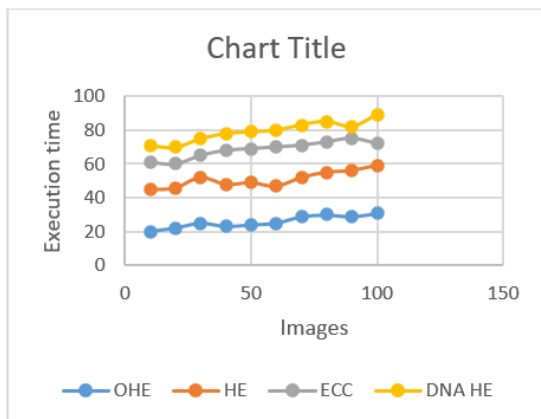

Figure 6. comparative analysis of execution time

Figure 6 shows a comparison of the proposed system to the current method at the time of implementation. When compared to the existing method, the new method's

implementation time is reduced. The DNA-HE algorithm reduces the implementation time of the recommended technique by 3%, while the ECC algorithm reduces it by 7%.

5. CONCLUSION

In this research, we propose a realistic web service architecture that uses DNA-HE to perform private detection utilizing knowledge operations on protected health information. The site host permits predictions despite just processing authorized data and understanding nothing about the highly confidential data provided. An efficient DNA homomorphic encryption technique is used to encrypt and store the data on the cloud. According to the trial's findings, the OHE algorithm reduced encryption time by 10%, the HE methods by 20%, and the ECC algorithms by 35%.

CONFLICTS OF INTEREST

The authors declare that they have no known competing financial interests or personal relationships that could have appeared to influence the work reported in this paper.

REFERENCES

[1] S.G. Sophia, "Secure Cloud Medical Data Using Optimized Homomorphic Encryption", *Turkish Journal of Computer and Mathematics Education (TURCOMAT)*, vol. *12*, no. 7, pp. 2702-2708, 2021. [Cross Ref] [Google Scholar] [Publisher Link]

[2] V. Pavithra, and C. Jeyamala, "A survey on the techniques of medical image encryption", In *2018 IEEE International Conference on Computational Intelligence and Computing Research (ICCIC)*, IEEE, pp. 1-8, 2018. [Cross Ref] [Google Scholar] [Publisher Link]

[3] S. Muthusundari, M.A. Berlin, R. Sasikumar, B. Alekhya, K. Mohanasundaram, and P. Prashant, "Transmitting data in a secure way using double protection encryption scheme", *Materials Today: Proceedings*. 2020. [Cross Ref] [Google Scholar] [Publisher Link]

[4] M. Marwan, A. Kartit, and H. Ouahmane, "Secure cloud-based medical image storage using secret share scheme," In *2016 5th International Conference on Multimedia Computing and Systems (ICMCS)* IEEE, pp. 366-371, 2016. [Cross Ref] [Google Scholar] [Publisher Link]

[5] E. Elmahdi, S.M. Yoo, and K. Sharshembiev, "Secure and reliable data forwarding using homomorphic encryption against blackhole attacks in mobile ad hoc networks", *Journal of Information Security and Applications*, vol. *51*, p.102425, 2020. [Cross Ref] [Google Scholar] [Publisher Link]

[6] S. Ullah, X.Y. Li, M.T. Hussain, and Z. Lan, "Kernel homomorphic encryption protocol", *Journal of Information Security and Applications*, vol. *48*, p.102366, 2019. [Cross Ref] [Google Scholar] [Publisher Link]

[7] J. Zhang, Y. Yang, Y. Chen, J. Chen, and Q. Zhang, "A general framework to design secure cloud storage protocol using homomorphic encryption scheme", *Computer*

Networks, vol. *129*, pp.37-50, 2017. [Cross Ref] [Google Scholar] [Publisher Link]

[8] J.H. Cheon, J. Kim, M.S. Lee, and A. Yun, "CRT-based fully homomorphic encryption over the integers", *Information Sciences*, vol. *310*, pp.149-162, 2015. [Cross Ref] [Google Scholar] [Publisher Link]

[9] R. Li, Y. Ishimaki, and H. Yamana, "Fully homomorphic encryption with table lookup for privacy-preserving smart grid", In *2019 IEEE International Conference on Smart Computing (SMARTCOMP)* IEEE. pp. 19-24, 2019. [Cross Ref] [Google Scholar] [Publisher Link]

[10] J. Li, J. Wu, G. Jiang, and T. Srikanthan, "Blockchain-based public auditing for big data in cloud storage", *Information Processing & Management*, vol. *57*, no. 6, p.102382, 2020. [Cross Ref] [Google Scholar] [Publisher Link]

[11] S. Velliangiri, and S. Alagumuthukrishnan, "A review of dimensionality reduction techniques for efficient computation", *Procedia Computer Science*, vol. *165*, pp.104-111, 2019. [Cross Ref] [Google Scholar] [Publisher Link]

[12] R.C. Williamson, B. Doiron, M.A. Smith, and M.Y. Byron, "Bridging large-scale neuronal recordings and large-scale network models using dimensionality reduction", *Current opinion in neurobiology*, vol. *55*, pp.40-47, 2019. [Cross Ref] [Google Scholar] [Publisher Link]

[13] Z. Wu, Y. Li, A. Plaza, J. Li, F. Xiao, and Z. Wei, "Parallel and distributed dimensionality reduction of hyperspectral data on cloud computing architectures", *IEEE Journal of Selected Topics in Applied Earth Observations and Remote Sensing*, vol. *9*, no. 6, pp.2270-2278, 2016. [Cross Ref] [Google Scholar] [Publisher Link]

[14] H.I. Kim, H.J. Kim, and J.W. Chang, "A secure kNN query processing algorithm using homomorphic encryption on outsourced database", *Data & knowledge engineering*, vol. *123*, p.101602, 2019. [Cross Ref] [Google Scholar] [Publisher Link]

[15] X. Wang, "One-round secure fair meeting location determination based on homomorphic encryption", *Information Sciences*, vol. *372*, pp.758-772, 2016. [Cross Ref] [Google Scholar] [Publisher Link]

[16] S.P. Raja, "Joint medical image compression–encryption in the cloud using multiscale transform-based image compression encoding techniques", *Sādhanā*, vol. *44*, no.2. p.28, 2019. [Cross Ref] [Google Scholar] [Publisher Link]

AUTHORS

S. Gnana Sophia is an Assistant professor of the Computer Applications Department at Scott Christian College, Nagercoil, Tamilnadu, India. She has received her Bachelor's degree in Computer Science from Women's Christian College, Nagercoil and a Master's degree in Computer Science from Srimati Indira Gandhi College Trichy, Tamilnadu. She has several years of work experience in the field of teaching and have arranged/organized many conferences, seminars, workshops and various other events. She has published many refereed journal articles/conference papers. Her research interest includes Cloud-based Encryption Technologies.

K. K. Thanammal received the M.Sc (Computer Science) Degree from Bharathidasan University, Tiruchirappalli in 1992, M.Phil (Computer Science) Degree from Manonmaniam Sundaranar University, Tirunelveli in 1999, M.Tech (Computer Science) Degree from Vinayaka Mission University, Salem in 2007 and Ph.D. (Computer Science) Degree from Manonmaniam Sundaranar University, Tirunelveli in 2015. She is working as Associate Professor in the Computer Science Department at S.T.Hindu College, Nagercoil since 1993. She has 27 years of teaching experience. She has published seven papers in journals and presented in seven National and International Conferences. Her current research interest focuses on Image Processing, Neural Networks, Medical imaging, and Cloud based Encryption Technologies.

S. S. Sujatha completed her MCA degree in Alagappa University, Karaikudi in 1993, M.Phil (Computer Science) Degree from Manonmaniam Sundaranar University, Tirunelveli in 2003, She completed her doctorate degree at Mother Teresa University, in 2014. She is working as Associate Professor in the Computer Science Department at S.T.Hindu College, Nagercoil since 1994. She has published eighteen papers in journals and presented in three International Conferences. Her current research interest focuses on Image Processing, Data Mining, Cloud Computing and Cloud based Encryption Technologies

RESEARCH ARTICLE

BRAIN ANEURYSM DETECTION VIA FIREFLY OPTIMIZED SPIKING NEURAL NETWORK

A. Jegatheesh[1, *], N. Kopperundevi[2] and M. Anlin Sahaya Infant Tinu[3]

[1]Assistant Professor, Department of Biomedical Engineering, SRM Institute of Science and Technology, Ramapuram Campus, Chennai, Tamil Nadu, India.

[2]Assistant Professor SG-2, School of Computer Science and Engineering, Vellore Institute of Technology, Vellore, Tamil Nadu, India.

[3]Research Scholar, Department of Electronics and Communication Engineering, Anna University, Chennai, Tamil Nadu, India.

[*]*Corresponding e-mail:abjegatheesh@gmail.com*

Abstract – **Aneurysms in the brain occur often; the frequency is around 4%. The mass effect is mostly responsible for the symptoms of unruptured aneurysms. The actual risk arises if the aneurysm bursts and results in a subarachnoid haemorrhage, though. The majority of aneurysms are asymptomatic and do not burst, although even minor aneurysms can do so due to the unpredictable growth of aneurysms. Imaging methods including intra-arterial digital subtraction angiography, computed tomography angiography, and magnetic resonance angiography are used to diagnose and track intracranial aneurysms. In this paper, a deep learning approach is proposed to detect and classify the brain aneurysm. Initially, the MRI images are skull stripped and the images augmented and reduce the noise using Kalman filter in the pre-process phase. The segmentation can be done by the firefly optimization algorithm. The segment nodules are classified into three classes by using the spiking neural network. The proposed model achieves the highest level of classification accuracy, which is 99.80%. As a result, when compared to other models currently in use, classification using BSF yields results that are much higher in efficiency and accuracy.**

Keywords – *Brain aneurysm, firefly optimization algorithm, Kalman filter, spiking neural network.*

1. INTRODUCTION

A brain aneurysm is a dangerously enlarged, blood-filled region of a weak or thinning blood vessel in the brain. A larger aneurysm increases the risk of rupture and subarachnoid haemorrhage (SAH) by compressing the surrounding neurons and brain tissue. The possibility of such a rupture is affected by the aneurysm size and shape [1]. Cutting the aneurysm neck is a viable surgical technique to stop rupture. Therefore, knowing the shape of a cerebral aneurysm is crucial for both identifying cerebral aneurysms and determining the position and posture of the required clips during diagnostic testing [2].

Some patients did not show cerebral bleeding despite having rupture aneurysms. On the other hand, it can be hard to identify which aneurysm ruptures in patients with numerous aneurysms, even though there is cerebral bleeding. Determining the condition of brain aneurysms accurately is therefore crucial for medical care and prognosis assessment [3,4]. While the treatment of aneurysms that have not ruptured is uncertain ruptured aneurysms require immediate surgery. Some unruptured aneurysms may never show symptoms [5], and problems might result from intravascular or microsurgical treatment. [6].

Brain aneurysms may be detected non-invasively, accurately, and reliably using computed tomography angiography (CTA) [7]. CTA demonstrated that a number of morphological characteristics, including diameter, aneurysm length, height, breadth, surface area, volume, etc., were related to aneurysm rupture when comparing the morphologies of ruptured and unruptured aneurysms. Other studies have demonstrated the value of using CTA images to classify ruptured and unruptured cerebral aneurysms using radiomics [8]. The following are the contributions of this research:

- The dataset used in this study, which includes training pictures of brain aneurysms, contains brain MRI scans.
- From the MRI images the skull stripped and the input images are augmented. By using this Kalman filter pre-process these MRI images to reducing the noise.
- The segmentation process can be done by using the Firefly optimization algorithm and the brain nodules are segment.

- The segmented brain nodules are taken as the input of the classification phase. That inputs are classified into three classes by using the spiking neural network such as Saccular Aneurysm (SA), Mycotic aneurysm (MA) and fusiform aneurysm (FA).

The remaining five portions of this paper were organised as follows. The literature review is presented in Section 2, the suggested approach for treating brain aneurysms using a spiking neural network and Section 3 introduces the firefly optimisation algorithm (BSF), Section 4 presents the findings and discussion, and Section 5 offers a conclusion.

2. RELATED WORK

Recently the researchers used a variety of deep learning and machine learning techniques mainly to improve the accuracy of detecting brain aneurysm from the MRI images. In this section, a few of those methods are studied shortly discussed.

In 2023 Xie, Y., et al., [9] employed a 3D convolutional neural network (CNN) encoder that automatically extracts complex hidden information. The best characteristics that are particularly relevant to the fracture risk data are found using the LASSO regression method, and a support vector machine (SVM) is employed to make the final fracture risk prediction. According to test findings, our classification approach can produce accuracy and AUC values of 89.78% and 89.09%, respectively.

In 2023 Regaya, Y., et al., [10] presented a technique for segmenting cerebral aneurysms in two dimensions using statistical and multiresolution methods. HMRF-EM (Expectation maximization in a hidden Markov random field) segments images based on spatial context restrictions while Contourlet Transform (CT) collects image features. The accuracy was attained 99.72%.

In 2023 Fujimura, S., et al., [11] created a machine learning model (MLM), In order to predict the ideal size and length of the first coil by gathering data on patients and aneurysms that had previously had successful coil embolization treatment. The accuracy rate of the prediction of size and length is 86.3% and 83.4% respectively.

In 2023 Ishihara, M.,et al., [12] evaluated the capability of convolutional neural network (CNN) scores features to distinguish between infundibular dilatation (ID) and an unruptured aneurysm (UAN). Using magnetic resonance angiography, we apply clinically available deep learning-based computer-aided diagnostic tools to identify unruptured aneurysms (UANs). Overall, the accuracy is 83.2%, specificity is 82.6%, and sensitivity is 89.0%.

In 2023 Niemann, A., et al.,[13] suggested a pipeline for analyzing cerebral aneurysms that includes automatic center line and outlet recognition, Segmenting networks using deep learning (MeshCNN) and generating semantic angiograms automatically. Morphological analysis with automatic injury status categorization and semantic

angiography. The 3D surface models may also be used to classify rupture states, which has an accuracy of 83.3%.

In 2023 Li, X., et al.,[14] proposed best machine learning approach to investigate the risk variables for Haemorrhagic transformation (HT) after Acute cerebral infarction (ACI) and create a model that can accurately assess both the likelihood of HT occurrence, it examines various machine learning methods. The HT risk prediction model developed by the XgBoost algorithm performed best, with an accuracy rate of 95%.

In 2022 Lei, X., et al., [15], A network based on the three-dimensional (3D) U-Net model was constructed, and the network was fed the collected image data in order to perform the automatic localization and segmentation of the aneurysm. In order to find and pinpoint potential aneurysm locations, the 3D convolutional neural network (CNN) network can extract the aneurysm blood vessels. The degree of accuracy is 97.19%.

Several machine learning and deep learning algorithms were developed from these related efforts with the goal of classifying brain aneurysms. By categorising brain aneurysms into three classes—saccular aneurysm, mycotic aneurysm, and fusiform aneurysm—the proposed BSF framework also aims to increase classification accuracy. The deep learning-based Firefly optimization algorithm is used for segmentation, in which spiking neural network employed for classifying the MRI images into three different classes with high accuracy to early detection of brain aneurysm.

3. PROPOSED MODELLING

In this section, we proposed a deep learning-based framework for classifying brain aneurysm into three classes from the MRI brain images. The figure shows the three steps of the proposed system. The Kalman filter is used to first eliminate the noise artefacts. Using the firefly optimisation approach, the pre-processed MRI images are used as an input for segmentation. Based on these segment nodules, a spiking neural network classifies the pictures as having saccular, mycotic, or fusiform aneurysms. The suggested BSF model's entire workflow is depicted in Figure 1.

3.1. Dataset

The brain MRI images were acquired from IntaA datasets. 103 Reconstructing the patient's scanned 2D MRA images yields 3D models of all the patient brain vessels. 1,909 vessel segments, including 215 aneurysm segments for diagnosis and 1,694 healthy vascular segments, are created automatically from the entire model. A medical expert manually splits and annotates 116 aneurysm segments. The requirement for preoperative examination determines the size of each aneurysm section.

3.2. Data Pre-processing Phase

In this paper the MRI images are preprocessing by using the Kalman filter for reduce the noise. The Kalman filter effectively manages uncertainty brought on by irregular external influences and noisy sensor data. Using

the projected system state and a weighted average, the Kalman filter generates an estimate of the system state from the average of fresh measurements. Equations 1 to 6 display the Kalman filter equations for the prediction steps.

$$\hat{a}_{\bar{k}} = L\hat{a}_{\bar{k}} + Mu_k + w_k \tag{1}$$

$$A_k = LLA_{k-1} + L^T + B \tag{2}$$

$$K_k = A_{\bar{k}}H^T(DA_{\bar{k}}D^T + C)^{-1} \tag{3}$$

where, $\hat{a}_{\bar{k}}$ is a vector prediction, $\hat{A}_k$ is the predictive covariance matrix and K_k is kalman gain. Next predictions are updated with measurements z_k

$$\hat{a}_{\bar{k}} = \hat{a}_{\bar{k}} + K_k(z_k - D\hat{a}_{\bar{k}}) \tag{4}$$

$$z_k = D\hat{a}_{\bar{k}} + v_k \tag{5}$$

Then the error covariance is update

$$A_k = (N - K_k D)A_k \tag{6}$$

Predictions about the upcoming condition will be made using the updated state variable. As many times as necessary for the needed time discretization, these processes will be repeated.
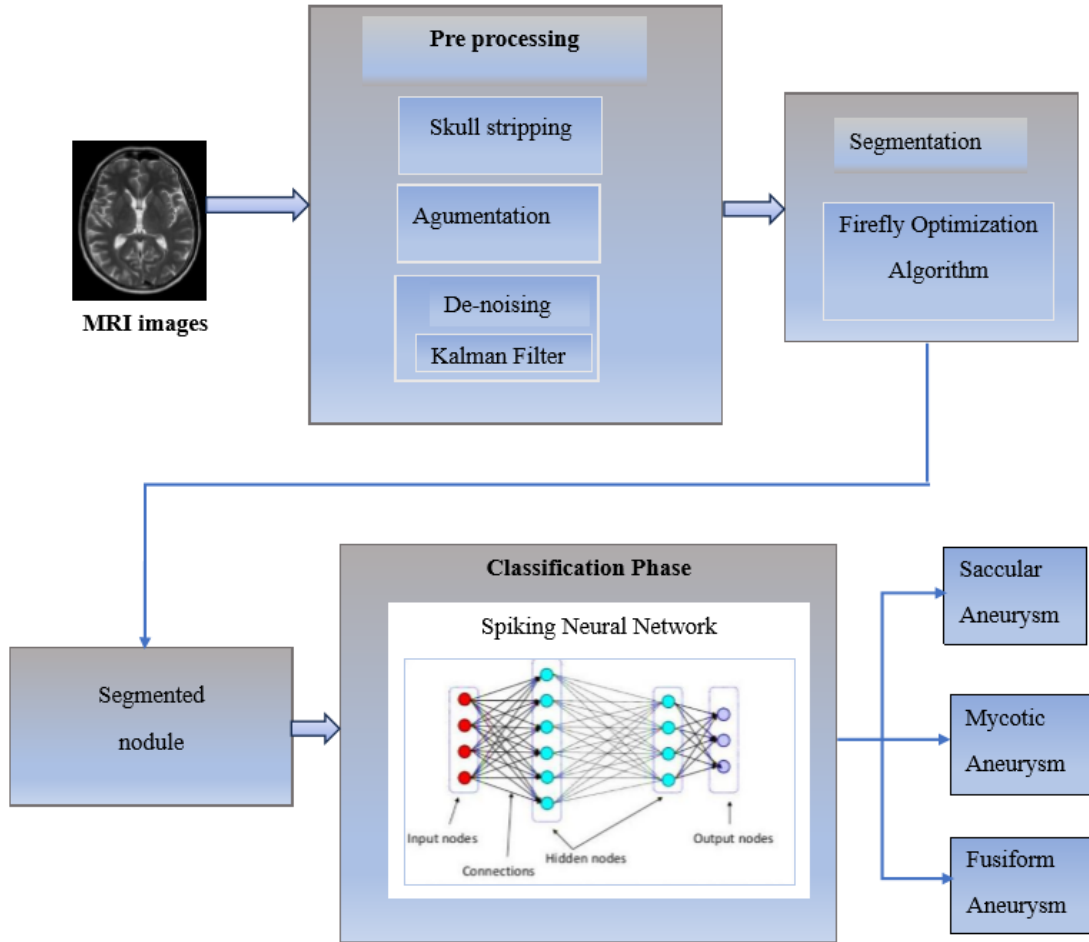

Figure 1. Proposed method working architecture

3.3. Segmentation Phase

The segmentation done by using the Firefly Optimization algorithm which affected by Firefly flickering behaviour. The patch is ultimately located using the algorithm left-to-right and top-to-bottom searches for the best matching patch. However, a lot of work and errors happen when there are numerous candidate fixes. To discover the best matching patch, a Firefly optimization technique was developed. Numerous applications have used the Firefly Optimisation technique to tackle a range of optimisation problems. Constrained, multi-criteria, and discrete optimization issues have all been addressed by Firefly Optimization algorithm.

Using the Firefly method, aneurysm affected portions are accurately identified in images, segmentation and class selection are optimized to recover the true aneurysm affected portion. The Firefly algorithm chooses appropriate features by examining the texture of image pixels. The Firefly algorithm processes for optimizing image segmentation are shown in Figure 2.

Image segmentation is optimized by the Firefly algorithm. Make a starting population of fireflies, specify the parameters for attraction, absorption, and selection, then make a new population and figure out the fitness function. The satisfaction criteria are examined following a number

of iterations, and if they are met, the preceding step or exit is chosen.

This algorithm development considers differences in brightness or light intensity in addition to the notion of attractiveness. A form of adaptive function is used to represent and quantify firefly brightness, with varied light intensities for various light sources. The intensity of the light affects brightness, which determines attractiveness. The following formula is used to determine each firefly level of attraction (7).

$$\beta(t) = \beta_0 e^{-\gamma t^2} \qquad (7)$$

where β_0 denotes the attractive force at distance (t) = 0, which in mathematical calculations can be treated as 1. The height of light absorption is denoted by the symbol. T represents the separation of two fireflies, i and j, located at various locations.
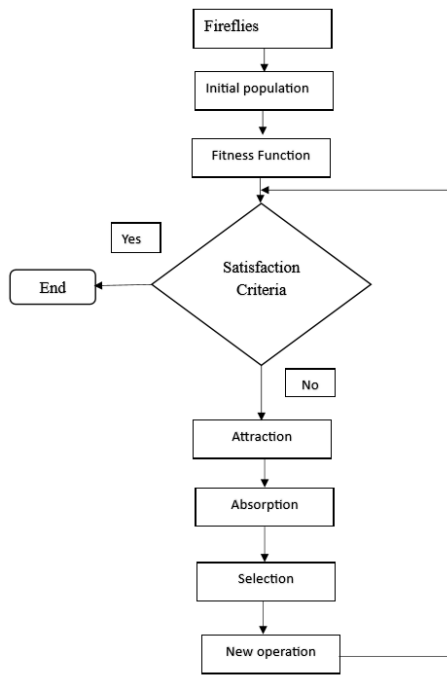

Figure 2. Firefly Algorithm flow diagram for optimization of image segmentation

Fireflies frequently change their locations. This shows that firefly' attraction to one another may be influenced by distance. As a result, the well-known Euclidean distance rule is used to calculate the distance between any two fireflies, i and j:

$$t_{ij} = |a_i - a_j| = \sqrt{\sum_{k=1}^{d}\left(a_{i,k} - a_{j,k}\right)^2} \qquad (8)$$

where d is the problem's size and a_(i,j) is the position of firefly i's k-th component. Assume that firefly i and firefly j are drawn to one another and move in that direction after determining the distance between the two fireflies. Equation (9) governs this kind of motion and is denoted by

$$a_i^{n+1} = a_i^n + \beta_0 e^{-(\gamma t_{ij}^2)} * \left(a_j^n - a_i^n\right) + \alpha * \left(rand - \tfrac{1}{2}\right) \qquad (9)$$

where n represents the number of iterations, coefficient the size of the random walk, and rand a random number generator that produces numbers between [0, 1]. After three words are weighed, low intensity fireflies turn into high intensity fireflies. The first word is the current position of the low brightness firefly. The second term is the movement by the attraction coefficient towards the firefly with higher brightness. In order to determine the final term, a random number generator is multiplied by a sort of random walk.

3.4. Classification Phase

The Spiki Neural Network classify the brain aneurysm into three different classes such as saccular aneurysm, Mycotic aneurysm and fusiform aneurysm. In a genuine neuron, the biophysical processes of potential creation on the neuron membrane are represented by differential equations that control impulse transmission. One of the most popular mathematical models for precisely simulating the biological function of the neuron is a leaky integrate-and-fire (LIF) neuron.

According to this model, the input L(t) is a voltage increase that updates the hidden state (membrane potential), M(t), which in turn causes spikes to appear in the output P(t). The membrane potential following the spike trigger is represented by N (t). These equations can be used to explain its behaviour.

$$M(t) = f (N (t-1), L(t)) \qquad (10)$$

$$P(t) = g(M(t) - Nthreshold) \qquad (11)$$

$$= \theta(L(t) - Nthreshold)$$

$$N (t) = L(t) (1 - P(t)) + NresetP(t) \qquad (12)$$

Nthreshold is the threshold for spike firing, L(t) is the input to the neuron at timestep t, Nreset is the potential to which the neuron returns following the spike, and so on. The neuron's state update equation is denoted by the notation f (N (t 1), L(t)). The update function utilised for the LIF neuron is as follows, where is a membrane time constant:

$$M(t) = f (N (t-1), L(t)) \qquad (13)$$

$$= N (t-1) - 1\,\tau ((N (t-1) + Nreset) + L(t))$$

The Heaviside step function $\theta(x)$, which has the following definition, is utilised for the spike generating function g(t):

$$\theta(x) = \begin{cases} 1, for\ x \geq 0 \\ 0, for\ x < 0 \end{cases} \qquad (14)$$

4. RESULTS AND DISCUSSIONS

The deep learning toolbox MATLAB 2019b was used to implement the experimental design of this work. The three kinds of brain aneurysms were classified using MRI images from the IntrA dataset in this outcome analysis. Utilising the particular characteristics, the suggested BSF approach's effectiveness is assessed. Additionally, a comparison of the proposed BSF framework to alternative models is presented.

4.1. Performance Analysis

In this subsection, the accuracy, specificity, precision, sensitivity, and F1 score of the proposed model were assessed. If a patient is healthy, it may be determined using the specificity. As a result, the specificity is established:

$$S = \frac{tn}{tn+fp} \tag{15}$$

The patient's sickness condition is determined by the sensitivity (or recall). By classifying the sample photos detected as true positives in the patients, it is utilised to assess the accuracy of the results. According to estimates,

$$R = \frac{tp}{tp+fn} \tag{16}$$

Where, precision is the characteristic of a successful model prediction and is obtained as,

$$P = \frac{tp}{tp+fp} \tag{17}$$

The representation of real positives and negatives as well as false positives and negatives is measured by the accuracy. It is employed to extract a certain characteristic from photos. The precision is evaluated using,

$$A = \frac{tp+tn}{total\ no.of\ samples} \tag{18}$$

$$F1 = 2\left(\frac{P*R}{P+R}\right) \tag{19}$$

Here, the terms true-positives, true-negatives, false-positives, and false-negatives of the samples are denoted by tp, tn, fp, and fn. The table.1 below displays the model's efficiency.

Table 1. Performance analysis of the proposed method

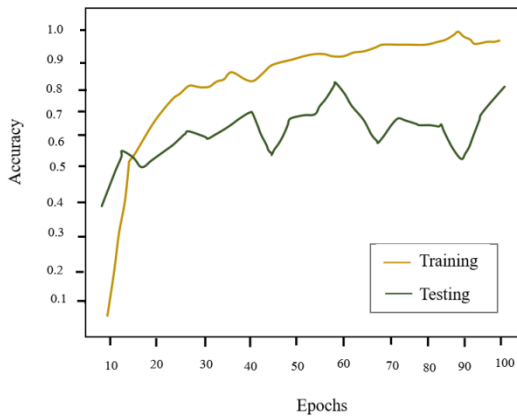| Class	Specificity	Sensitivity	Precision	F1 score	Accuracy
Saccular aneurysm	99.12	99.04	98.23	99.12	99.80
Mycotic aneurysm	98.20	98.13	97.42	98.74	99.82
Fusiform aneurysm	99.67	99.57	99.76	99.43	99.79

Figure 3. Training and Testing accuracy curve for 3-class classification

The F1 score, specificity, precision, sensitivity, and accuracy were the key characteristics used to evaluate the effectiveness of the suggested BSF framework. Table.1

shows the performance evaluation based on the datasets for the saccular, mycotic, and fusiform classes. The saccular aneurysm (SA), mycotic aneurysm (MA), and fusiform aneurysm (FA) are all accurately identified using this model.

According to the accuracy curve in Fig. 3, which plots accuracy on the y-axis and epochs on the x-axis, the technique's accuracy rises as the number of epochs is increased. The loss of the model diminishes as the number of epochs grows, as seen in Fig. 4's epoch vs loss graph. The BSF model successfully and precisely divides things into three groups
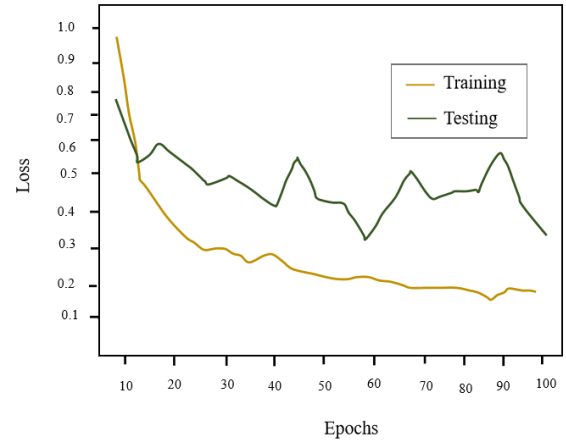

Figure 4. Training and Testing loss curve for 3-class classification
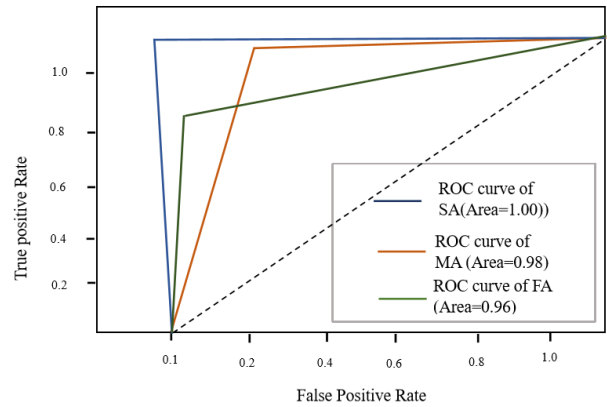

Figure 5. ROC curve for three class classification

Figure 5 shows the ROC calculated for the datasets of MRI images. The TPR and FPR metrics may be used to measure the suggested BSF approach's higher AUC of 0.998 for the 3-class. The suggested model has a 99.80% overall accuracy for three classes.

4.2. Comparative Analysis

In order to confirm that the outcomes of the suggested BSF model attain high accuracy, the effectiveness of each approach was estimated.

The suggested model was evaluated in comparison to four existing approaches, including SVM, CNN, XG Boost, and MRF. The proposed BSF outperformed the other approaches with an accuracy of 99.80%, which was measured using a range of criteria, including specificity,

sensitivity, f1 score, and accuracy. Based on table.2's performance parameters for identifying cervical cancer and obtaining the necessary percentage of classification accuracy, a comparison of several techniques was made. The proposed BSF uses MRI scans to predict brain aneurysms with a total accuracy of 99.80%. However, as compared to the BSF classifier, older methods did not perform as well. In comparison to SVM, CNN, XG Boost, and MRF, the BSF model improves overall accuracy range by 10%, 16.6%, 4.8%, and 0.1%, respectively.

Table 2. Comparison between other methods

Methods	Specificity	Sensitivity	Accuracy
SVM	87.2	88.6	89.8
CNN	84.6	83.8	83.2
XGBoost	94.2	95.8	95.0
Markov Random Field (MRF)	98.8	99.4	99.7
Proposed model	99.2	99.7	99.8

According to the comparison above, the BSF is more accurate than the current models. In order to increase the accuracy of diagnosis, a three-class classification model will be trained in the future. It will properly anticipate the phases of aneurysm. To make the suggested model more useful and practical, it was also trained on data from other areas, such as colposcopy samples. Performance comparison of four classifiers shown in Figure 6.
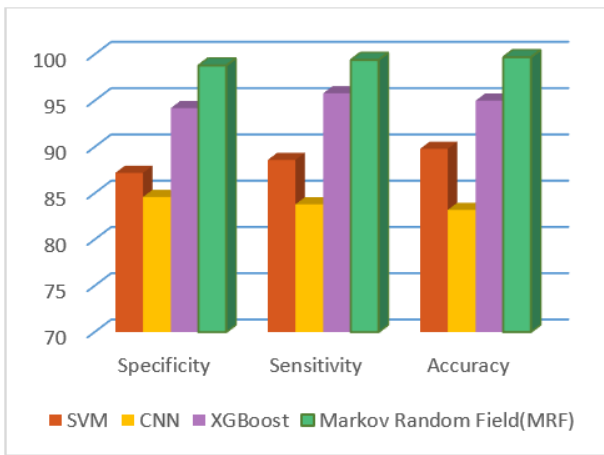

Figure 6. Performance comparison of four classifiers

Table 3. Comparison between proposed and existing models

Year & Author	Model	Accuracy (%)
2023, Xie, Y [9]	SVM	89.8
2023, Ishihara, M [12]	CNN	83.2
2023, Li, X,[14]	XGBOOST	95
2022, Lei, X,[15]	MRF	98.7
Proposed	BSF	99.8

The proposed BSF technique produces results with more accuracy than the cutting-edge approaches, according to the comparison in table.3 above. The suggested BSF model successfully predicts cervical cancer using MRI images with an overall accuracy of 99.8%. However, in comparison to the suggested BSF framework, the current frameworks did not perform well. The suggested model outperforms SVM [9], CNN [12], XGBoost [14] and MRF [15] in terms of overall accuracy by 10%, 16.6%, 4.8%, and 0.1%, respectively. In categorizing the various MRI images, the suggested BSF model outperforms to produce superior classification outcomes.

5. CONCLUSION

This study used MRI scans from IntrA datasets to create a deep learning framework for predicting brain aneurysms. The Kalman filter lowers the distortion noises in the photographs. Therefore, the MRI images are classified using the Spiki Neural Network into saccular aneurysms (SA), mycotic aneurysms (MA), and fusiform aneurysms (FA). Thus, the outcome shows that the suggested method can categorise the MRI images for the purpose of identifying brain aneurysms. The suggested approach outperforms while maintaining a 99.8% accuracy range. Conclusion: The proposed framework outperforms other existing models in terms of accuracy on both training and testing datasets. This method can boost detection rates, enabling quick and accurate clinical treatment.

REFERENCES

[1] T.H. Champney, Essential clinical neuroanatomy. John Wiley & Sons. 2023. [CrossRef] [Google Scholar] [Publisher Link]

[2] A. Alaraj, "Virtual reality cerebral aneurysm clipping simulation with real-time haptic feedback", *Neurosurgery,* Vol. 11, No. 1, pp. 52–58, 2015. [CrossRef] [Google Scholar] [Publisher Link]

[3] S.N. Ahmed, and P. Prakasam, A systematic review on intracranial aneurysm and hemorrhage detection using machine learning and deep learning techniques. Progress in Biophysics and Molecular Biology, 2023. [CrossRef] [Google Scholar] [Publisher Link]

[4] B. Kranawetter, M. Hazaymeh, D. Mielke, V. Rohde, and T. Abboud, missing a Blood Blister-Like Aneurysm in the Setting of Aneurysmal Subarachnoid Hemorrhage in a Patient Harboring Multiple Aneurysms. Stroke, 54(9), pp. e434-e437. 2023. [CrossRef] [Google Scholar] [Publisher Link]

[5] T.N. Nguyen, Management of Unruptured Intracranial Aneurysms and Brain Arteriovenous Malformations. CONTINUUM: Lifelong Learning in Neurology, 29(2), pp.584-604, 2023. [CrossRef] [Google Scholar] [Publisher Link]

[6] O. N. Naggara, "Endovascular treatment of intracranial unruptured aneurysms: systematic review and meta-analysis of the literature on safety and efficacy", *Radiology,* vol. 256, pp. 887–897, 2010. [Cross Ref] [Google Scholar] [Publisher Link]

[7] R. S. Bechan, "CT angiography versus 3D rotational angiography in patients with subarachnoid hemorrhage", *Neuroradiology,* vol. 57, pp. 1239–1246, 2015. [CrossRef] [Google Scholar] [Publisher Link]

[8] Y. Xie, "Automatic risk prediction of intracranial aneurysm on CTA image with convolutional neural networks and radiomics analysis", *Frontiers in Neurology*, vol. *14,* 2023. [CrossRef] [Google Scholar] [Publisher Link]

[9] Y. Regaya, "Development of a cerebral aneurysm segmentation method to prevent sentinel hemorrhage", *Network Modeling Analysis in Health Informatics and Bioinformatics*, vol.*12*, no. 1, p.18, 2023. [Cross Ref] [Google Scholar] [Publisher Link]

[10] S. Fujimura, "Development of Machine Learning Model for Selecting the 1st Coil in the Treatment of Cerebral Aneurysms by Coil Embolization", 2023. [Cross Ref] [Google Scholar] [Publisher Link]

[11] M. Ishihara, "Detection of intracranial aneurysms using deep learning-based CAD system: usefulness of the scores of CNN's final layer for distinguishing between aneurysm and infundibular dilatation", *Japanese Journal of Radiology*, vol 41, no. 2, pp.131-141, 2023. [CrossRef] [Google Scholar] [Publisher Link]

[12] A. Niemann, "Deep learning-based semantic vessel graph extraction for intracranial aneurysm rupture risk management". *International Journal of Computer Assisted Radiology and Surgery*, vol. 18, no. 3, pp.517-525, 2023. [Cross Ref] [Google Scholar] [Publisher Link]

[13] X. Li, "Machine learning predicts the risk of hemorrhagic transformation of acute cerebral infarction and in-hospital death". *Computer Methods and Programs in Biomedicine*, vol. *237*, p.107582, 2023. [Cross Ref] [Google Scholar] [Publisher Link]

[14] X. Lei, "Deep Learning-Based Magnetic Resonance Imaging in Diagnosis and Treatment of Intracranial Aneurysm". *Computational and Mathematical Methods in Medicine*, *2022*. [Cross Ref] [Google Scholar] [Publisher Link]

[15] B. Wang, "A modified firefly algorithm based on light intensity difference", *Journal of Combinatorial Optimization*, vol. 31, pp.1045-1060, 2016. [CrossRef] [Google Scholar] [Publisher Link]

AUTHORS

A. Jegatheesh received the B.E degree in Electronics and Instrumentation Engineering from Noorul Islam College of Engineering affiliated to Anna University and M.E degree in Applied Electronics from Annna University Regional Campus-Tirunelveli. He received his Ph.D. degree in Information and Communication Engineering from Anna University Chennai, India. Currently he is doing as as an Assistant Professor in Arunachala College of Engineering for Women, Kanyakumari, Tamilnadu. His research area includes Control Systems, Process Control, Image Processing, Signal Processing.

N. Kopperundevi is currently working as Assistant Professor at Vellore Institute of Technology Vellore. She completed her research the year 2019 under Anna University Chennai, in the specialisation of Information Communication Engineering. She has published more than 10 papers and three patents. Acting as a reviewer in Textile Research Journal and Soft Computing has reviewed nearly 10 papers. Her area of interest includes Image Processing, Neural Networks, Fuzzy Systems Machine Learning and Deep Learning and have guided more than 15 UG and PG projects.

M. Anlin Sahaya Infant Tinu is doing her Ph.D research from Anna University, India. She had been working as Assistant professor in A.R. College of Engineering and Maria college of engineering, India. She is now actively doing her research on "Brain Tumor Detection Using Deep Learning Techniques" under the guide ship of Dr. Ahilan Appathurai, Associate Professor in the department of electronics and communication engineering at PSN college of engineering and technology, India. She has attended International Conference on trends in engineering organized by Arunachala College of Engineering for Women, India. She has presented a paper "Automatic Segmentation of Brain Tumor in MRI Images". She also has been a student member of IEEE for three years and actively participated in all the events conducted by IEEE Student Branch-62851.

RESEARCH ARTICLE

PRIMARY OPEN-ANGLE GLAUCOMA SEVERITY PREDICTION USING DEEP LEARNING TECHNIQUE

Dr. A. Prasanth[1, *] and Dr. N. Muthukumaran[2],

[1]Assistant Professor, Department of Electronics and Communication Engineering, Sri Venkateswara College of Engineering, Sriperumbudur, Tamil Nadu, India.
[2]Professor, Centre for Computational Imaging and Machine Vision, Department of ECE, Sri Eshwar College of Engineering, Coimbatore, Tamil Nadu, India.
*Corresponding e-mail: draprasanthdgl@gmail.com

Abstract – **Glaucoma is a neuro optical disorder that lead to blindness over a period of time. In recent years, studies have revealed that diabetic patients are more common victims of glaucoma. The present research aims to investigate the relationships between intraocular pressure (IOP), refractive error, and primary open-angle glaucoma (POAG) in the wheatish population. Population-based research provide important information on the prevalence and hazards for glaucoma, such eye refractive defects. At low IOP stages, the correlation between glaucoma and myopia is strong, and it gradually decreases as IOP rises. A Deep learning tool is developed to analyze the severity of glaucoma using fundus image. According to this research, the association between IOP and glaucoma is strong at low mean values of 15±3.23 level and gradually weakens as IOP increases in the wheatish population, reaching 17.59±3.33 for PACG, 18.85±1.20 for POAG, 18.59±2.52 for PIGM, and 19.12±1.42 for OH. With increasing IOP, the glaucoma image in myopic eyes degraded, and no correlation with IOP ≥35 mmHg has been found.**

Keywords – *Refraction Error, Populace-based Study, POAG, Wheatish population, Deep Learning, Glaucoma.*

1. INTRODUCTION

Glaucoma is a neurological degeneration of optical cells that emerge due to multiple optical disorders. Generally, glaucoma is termed as "Silent thief of vision" as it gradually dwindles sight without any primary symptoms. Refractive error and Intra Ocular Pressure (IOP) are significant risk influences for POAG, and the commonness of refractive error is ascending over the world, indicating that plays a significant part in the improvement of POAG. Diplopia, haziness, glare or halos around bright lights, squinting, headaches, blurred vision, and eye strain are the most common recognized manifestations of refractive error (RE). Glaucoma is an unpredictable sickness that causes destruction to the optic nerve and prompts dynamic, irreversible vision calamity. It is the second main problem that can lead to blindness globally [1,2]. The optical field test, optic nerve imaging, corneal thickness and point checks, and

the eye weight examination are all types of glaucoma eye tests. The main role of RE in the etiology of glaucoma has play a significant role in glaucoma detection. This prompts to a condition referred Diabetic Retinopathy. The unending entanglements of diabetes related to eye infection is given in fig.1. Among these chronic complications, Diabetic retinopathy is an important reason for blindness in Indian adults. In some human beings with diabetic retinopathy, retinal blood vessels may also swell and outflows fluid. 1.8 million (4.8%) of the 376 million individuals are visually impaired because of eye infections all through the world. Globally around 171 million diabetes patients are there, and it is expected to 367 million at the end of 2030. About half of the persons with diabetes are unconscious, albeit around 2 million died consistently are owing to complexities of diabetes.
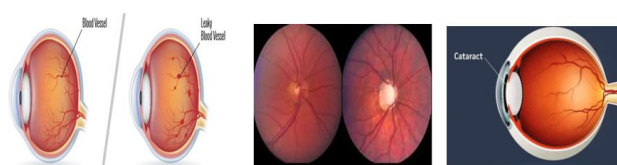

Figure 1. a) Diabetic Retinopathy b) Glaucoma c) Cataract

In the next 20 years, over 75% of patients is expected to have some type of diabetic retinopathy [3]. Glaucoma Research Foundation (GRF) conducted a review and discovered that, 74% of quite 1,000 people met afore mentioned criteria and their eyes must be tested at regular intervals and 61% of those with enlarged eyes were identified to have glaucoma. 16% of African Americans were reported to have recently affected with glaucoma [4,5]. Comprehensively, 1.31 billion people worldwide are thought to have some form of blindness. Additionally, 188.4 million people have mild vision disability, 216 million had modest to extreme vision hindrance, and 36 million people are visually

impaired [6]. Regarding close vision, 827 million people living with a close vision weakness [7].

In this paper, a huge populace overview has been performed so as to distinguish patients with undetected glaucoma. The subsequent material, comprising of in excess of 4000 people among Wheatish populace. The reason for the present examination is to contemplate the connection among RE and glaucoma, all the more explicitly to see whether nearsightedness can be affirmed as a significant hazard factor for glaucoma, and the relationship among myopia and glaucoma depend on IOP. Here a deep learning tool is implemented to evaluate the refractive error using the fundus image obtained from the survey among wheatish people. The ametropic condition (refractive index of light) of the eye were calculated to evaluate the occurrence of glaucoma.

This paper is organized in the following manner: In Chapter 2, a summary of the research is presented. Chapter 3 provides a description of the resources and procedures. The experiment's outcomes and insights are presented in Chapter 4, which also serves as the conclusion of the research.

2. REVIEW OF LITERATURE

Numerous elements have recently been accounted to influence IOP. A higher IOP was reported to be associated with greater central corneal thickness [8], blood pressure [9], and body mass index [10]. It has also been stated that the existence of diabetes mellitus was a hazard factor for high IOP. Because these confirmations are the most part of dependent on cross-sectional investigations which can't exhibit temporal causation, it is important to assess their relationship with IOP longitudinally.

The relationship among RE and glaucoma subtypes with 95% confidence intervals (CIs) measured as odds ratios (ORs). Myopia was related with an expanded occurrence of all types of POAG and OHTN, while hyperopia is related significantly to PACG occurrence.

While higher myopia was a strong hazard factor for subtypes of glaucoma, low and medium myopia often affects the risk of glaucoma. Also, there were significant racial differences in the correlation of myopia with the danger of POAG and NTG [11].

In [12], researchers examined the connection among refractive mistake, glaucoma, and IOP in a specific white community and discovered an overall link between myopia and high IOP and common glaucoma. In [13], evaluated primary congenital glaucoma (PCG)-related refractive results of cataract surgery with intraocular lens (IOL) implantation. After IOL implantation, there was a bigger myopia shift in the PCG eyes as well as a larger error in forecasting. Since their variations in axial dimension become more sensitive to IOP fluctuations, the eyes of kids with PCG are more vulnerable to optical abnormalities.

One study thought about the eyes that have undergone phacoemulsification with eyes that have not experience glaucoma surgery at least 3 months after trabeculectomy and revealed that the adjustment in IOP was adversely related with refractive surprise; a connection was expected among

lower postoperative IOP or greater reduction in IOP and reduction in axial length [14]. What's more, an ongoing report has uncovered that combined versus subsequent trabeculectomy, the refractive result was lower [15]. Then again, there were no differences in refractive and visual results in a study involving combined trabectome-cataract surgery with cataract-alone surgery, and a retrospective analysis demonstrated favorable refractive results in patients experiencing concurrent cataract removal with trabeculectomy or glaucoma drainage system surgery.

There are few population-based studies have been directed outside the USA or UK that inspected the frequency of DR, in which patients who were resolved to have diabetes from 1980 to 1984 had a 47% reduction in the risk of DR compared to patients analyzed from 1975 to 1979[16]. The diminishing in risk was significantly more unmistakable in the associate broke down from 1985 onwards, at 64 %. This assessment shows that while virtually all patients with type 1 diabetes may eventually make DR after some time, the frequency of type 1 diabetes patients with DR was undoubtedly on the decline. A population-based study between the wheatish population-Diabetic individuals was directed in this paper to discover the relationship between Refractive Error, IOP, and Glaucoma Etiology. A deep learning tool is implemented to evaluate the refractive error

3. PROPOSED METHODOLOGY

The proposed work is a population-based study of optical disorder in people with diabetic mellitus. The objective of the study is to evaluate the relationship of intraocular pressure, refractive error and the etiology of glaucoma among diabetic patients of wheatish populace. In this work, a survey is conducted among both men and women (age $\geq$ 40) with the history of diabetics. Along with a free eye test, it included a brief assessment about any previous eye conditions and current drugs.

3.1 Study Population

The targeted individual number is 4000 with the age group of greater than 40 years with male and female diabetes. The workflow diagram of this study is given in fig.2. Here, totally 4529 individuals have been investigated from 2018. In that 529 individuals have been excluded due to certain reasons which includes people aged less than 40 years, some of the individuals are already diagnosed their eye disease and are non-diabetic. Visual and refraction test have been performed on the identified individuals. If the individuals have clear vision, they are excluded from the study. Then the identified individuals are checked for blood pressure, eye tension and sugar test. Based on the testing results, final diagnosing has been 5.

3.2 Evaluation of Refractive error and Intraocular Pressure

The refractive status is obtained using a standardized automated refractor. As part of an ophthalmologic test, participants underwent perceptual refractive and also color fundus images at baseline and following visits. In addition, retinoscopy was used in the refraction protocol and then further refining of subjective refraction. Thirty-five-degree

field color fundus images were obtained using a reading center-approved reflection film using a fundus camera [17]. The equivalent macula-centered images were used in this analysis for each visit in which refraction was done. Based on baseline refraction, the refractive status of a specific eye was determined. Spherical equivalent (SE) of +1.00 D or below is Myopia (nearsightedness), SE of +1.00 D or above is hyperopia (farsightedness) and SE between -0.75 and +0.75D is emmetropia [18].
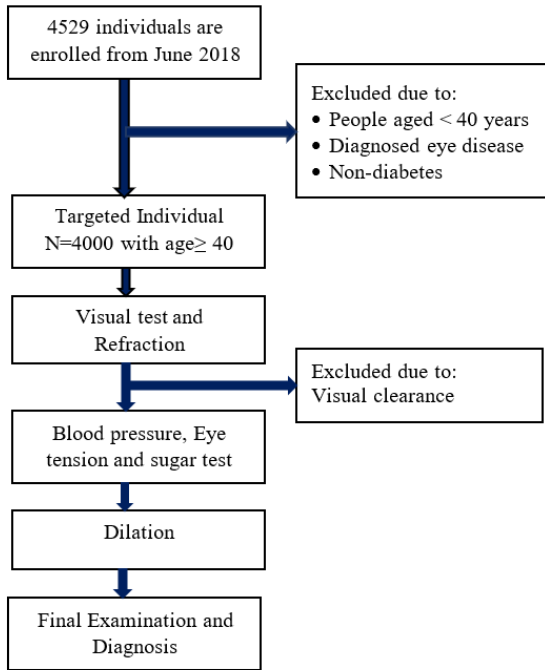
Figure 2. Work flow of Study population

Each subject has a visual field as part of the baseline study. After the threshold is defined, the analysis was conducted within the central 25 ° of the visual field using patterns of two, three or four stages (26 stimuli in all). If at the first attempt any point was not shown, it was retested, with any point twice missing on three attempts identified as a reported miss, constituting a screening test loss [19]. Subjects who lost in screening test underwent full perimetric testing of central visual field and only the threshold is analyzed those passed in screening test.

The IOP is measured using applanation tonometry followed by instilling a drop of tropicamide (dilation eye drop). During the dilation period the patient is enquired regarding their visual condition, occurrence of glaucoma and medication process. Images of the fundus and lens were taken for affected patients. The obtained data is trained and tested using a deep learning tool to determine the severity of POAG [20].

3.3. Implementation of Deep learning algorithm

The Fundus images taken from the patients were trained and tested to analyze the occurrence and severity of Diabetic Glaucoma among Wheatish populace. A Deep Convolution neural network classifiers is designed for automatic detection and classification of the medical diseases. Multiple convolutional layers, pooling layers, and fully linked layers often make up a DCNN. The RGB Fundus image is considered in this work to the output process of proposed retinal fundus image is evaluated through several steps such as preprocessing, feature extraction and classification are illustrated as follows;
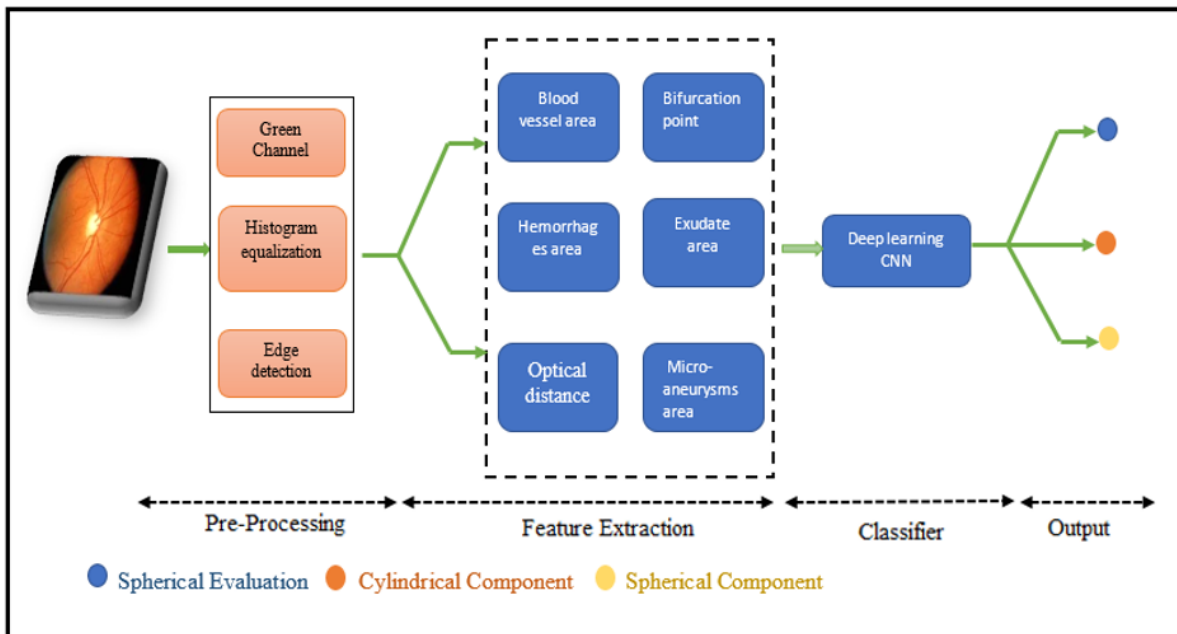

Figure 3. Block diagram of proposed deep learning technique

3.3.1. Pre-processing

Image preprocessing is a significant step to reduce the noise distortion and enhance image. It is an essential process that simplify the process of classification. In the proposed method preprocessing enhance the colour fundus image obtained from the patients in three steps. Green channel isolation, histogram equalization and edge detection.

Green Channel

The RGB fundus image has three colour channels (Red, Green and Blue). Here the Green channel (GC) manifests the contrast between exudates area, hemorrhages area, blood vessels and bifurcation point. Unlike the other two, green channel is neither low-illuminated nor high-saturated. Therefore, in this process only the green channel is extracted for classification of glaucoma.

Histogram equalization

Image Contrast is enhanced to elevate the features of the image. Histogram equalization is implemented to equalize and contrast the image. The images are segmented into small blocks and contrast is efficiently applied based on the intensity value of pixel. It enhances the contrast of local area to gain high contrast [21].

Edge detection

The enhanced images were resized and cropped as to make it standardized. Canny edge detection algorithm is used for edge detection where Gaussian filter smoothen the boundaries and gradient intensity is calculated to detect the edges.

3.3.2 Feature extraction

The preprocessed fundus image of the patients is subjected to feature extraction to analyse the exudate area. Feature extraction is olates all features from the fundus image to evaluate the exudate area; optical disc is removed as it develops similar colour and intensity to other features of retinal fundus image. The optical disc is generally removed by elevating the contrast around the optical disc. The blood vessels inside the optical disc can be removed by applying a Grayscale closing technique. In this study, optical features such as blood vessels, hemorrhage, bifurcation point, optical distance, micro aneurysms area and exudate area were isolated from the fundus image [23].

Figure 4. Optical Disc Elimination

The features extracted from the fundus image provides clear information for analytical study of glaucoma.

Optical blood vessels underneath the conjunctiva are subtle and may breakdown cause irritation and redness in eye resulting in sub conjunctival hemorrhage, if it is untreated that leads to retinal glaucoma. Similarly, the optical distance and bifurcation point provides detailed view of optical nerves. That simplify the isolation of extrude area. The extracted features were classified based using deep neural network.
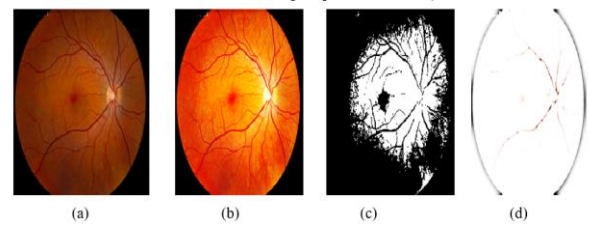

Figure 5. Extracted features of retinal fundus image. (a) Input fundus image, (b) Blood vessels, (c) bifurcation point and optical distance and (d) Micro aneurysm and exudate area.

3.3.3 Deep neural network

The categorization of health-related images is made easier by the multi-layered network approach known as deep neural networks. The initial data for a DNN network consists of training and test sets. Verification data from the training set was created using a DNN parameter with randomized thresholds set. The neural network is then fed the sample source image, and it compares and predicts the missing section based on the intensity of each pixel of the fundus image in the training set.
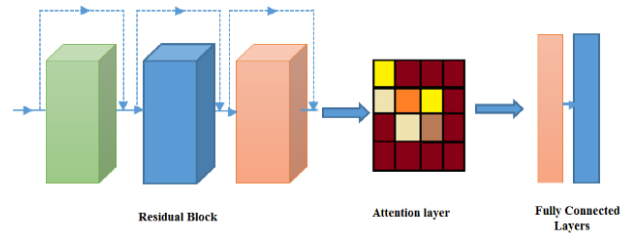

Figure 6. Architecture of Deep Neural Network

To effectively train a data set for forecasting glaucoma, this procedure is repeated with various fundus images [22]. The DNN design of our suggested approach uses a residual block, an attention layer, and A fully linked layer needed to understand the features of the retinal.

The residual block estimates the features extracted from the fundus images. The attention layer grasp more crucial features of images and the FC layers compare the extracted features with trained dataset.

The convolution layer containing three remaining components makes up the remaining network. The neural network's forward-feedback layers are what residual units are simple. For learning tiny parameters that reduce error, the residual unit has a bottleneck design of several convolution neural networks. In the ResNet design, a steady reduction in error is achieved by expanding the training layer. The precise traits are chosen by the layer of attention. Following the attention layer comes the layer that is totally connected, and the output is created utilizing the fundus image's spherical and cylindrical attributes.

4. RESULTS AND DISCUSSIONS

The commonness of glaucoma in screened subjects are arranged in table.1 at the hour of the screening assessment, all members were somewhere in the range of 40 and 78 years old. We distinguished 742 people with beforehand undiscovered essential open edge glaucoma (POAG),

ordinary strain glaucoma (NTG), essential point conclusion glaucoma, pigmentary and visual hypertension (OH) relating to 18.55% of those screened. We found an extra 268 people with glaucoma who had been recently determined and 23 people to have different kinds of glaucoma.

Table 1. Frequency of glaucoma in screened subjects

|	N (subjects)	%
Patients with detected glaucoma	742	18.55
Early diagnosed glaucoma patients	268	6.7
	23	0.57
Angle closure glaucoma patients Normal	2,967	74.17
Total	4,000	100

A total of 1,484 eyes are comprised in the present investigates, amongst them 1,216 (81.94%) are glaucoma eyes. In that, 598 right eyes and 618 left eyes. We excluded 268 (18.05%) cases which are unable to obtain pictorial acuteness, visual clearance, and eyes that had before experienced cataract operation and the details are tabulated in table.2.

The connection among the glaucoma and RE is detected in both males and females (fig.7 (a)), and across the age group is shown in fig.7 (b). We found a solid relationship among glaucoma and myopia, but also a strong reliance on IOP for the relationship. With rising IOP, glaucoma over-representation in the myopic group deteriorated slowly. There was a striking, practically straight connection among the occurrence of glaucoma with IOP ≤20 mmHg (Fig. 8) which occurred entirely in the eyes with IOP ≥35 mmHg and this distinction shows the huge connection among IOP and

RE. The association is good at minor IOP levels and completely vanished at higher IOP levels indicates that for normal stress glaucoma, myopia was an important risk factor.
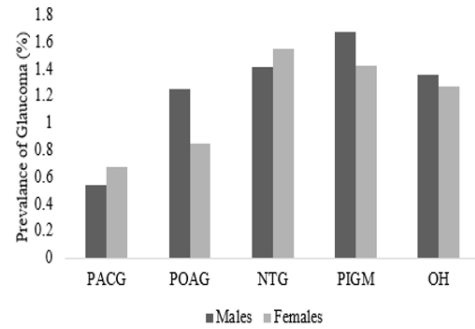
a) RE for males and females
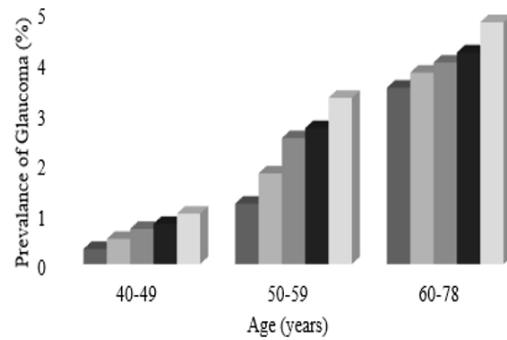
b) RE with age groups

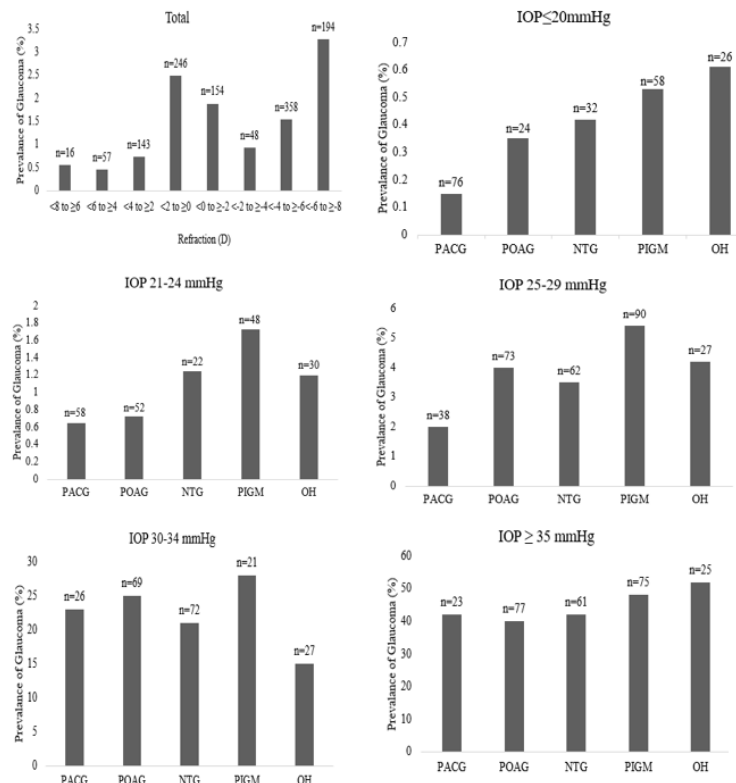**Figure 7.** Frequency of glaucoma in eyes

Figure 8. Frequency of glaucoma in eyes with various RE and IOP-levels

Table 2. Number of eyes (both left and right) involved in this paper

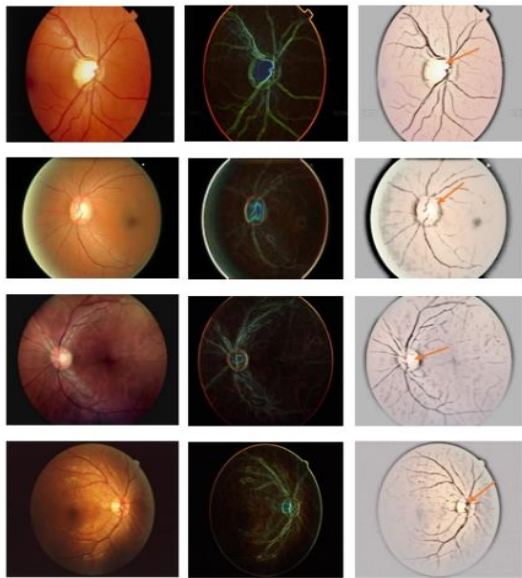|	N (eyes)	%
Overall quantity of eyes tested	1,484	
non-eligible	268	18.05
IOP≤25 mmHg eyes are eligible glaucoma	785	52.89
IOP>25 mmHg eyes are eligible glaucoma	431	29.04

Figure 9. Experimental result of fundus images trained through deep learning network to predict severity of primary open-angle glaucoma in diabetics among Wheatish populace.

Table 3 gives the highlights of the 5-glaucoma case and non-glaucoma controls. Glaucoma patients with ≥40 years with diabetic patients have been considered for this trial. Ladies set up 62% of controls, 71% of PACG patients, 56% of POAG, 49% of PIGM and 69% of OH with diabetic patients.

For men 59% of controls, 37% of PACG patients, 56% of POAG, 62% of PIGM and 44% of OH independently. The regularity of glaucoma subclasses is moved by race and ethnicity. Clinical incorporates moreover fluctuated with the subclasses of glaucoma. True to form, glaucoma cases commonly greater CDRs and greater IOPs than controls. Similarly, the diabetics by and large have higher estimation of IOP, lower estimation of CDR, and higher estimation of RE, however various patients had respectably lower estimation of IOP, higher estimation of CDR, and lower estimation of RE.

4.1 Experimental Analysis

Retinal fundus image taken from the patient is trained using a deep learning algorithm to evaluate the severity of glaucoma among Wheatish populace. The investigation evaluation of the fundus image is given below.

In experiment result, the fundus images obtained from patients with glaucoma is tested using the deep neural network where the images are classified based on the spherical and cylindrical components. The features of optical disc and optical cup are calculated. The spherical equivalent worse than -0.6 (myopic), spherical equivalent between -1.0 and+1.0 (Neutral) and spherical equivalent worse than 5.0 (hyperopic) are analysed to evaluate the occurrence and severity of POAG. From the analysis the DNN classification technique.

Table 3. Features of Glaucoma and controls for Wheatish population

	Controls	PACG	POAG	NTG	PIGM	OH
Gender						
Female	62.25	71.23	56.34	58.69	49.64	69.48
Male	58.95	36.92	56.34	48.64	62.76	44.68
Age						
40-49	27.30	4.29	6.14	5.89	13.79	11.32
50-59	40.10	28.36	31.40	32.59	43.69	40.69
60-78	32.50	65.89	62.50	62.25	45.95	51.69
Mean±SD	57.28 ±13.5	67.27±10.65	68.51±10.38	67.58±9.68	63.89±12.21	65.58±13.50
CDR						
Mean±SD	0.31±0.13	0.45±0.11	0.56±0.23	0.64±0.19	0.51±0.25	0.45±0.36
IOP						
Mean±SD	15.98±3.23	17.59±3.33	18.85±1.20	14.58±3.273	18.59±2.52	19.12±1.42

In India, 4.042 million with the age gathering of 40-49 years and 30.970 million with more noteworthy than 50 years are influenced from uncorrected refractive error [16]. The average IOP is 15.61 ± 3.09 mm Hg for women and 15.54 ± 3.54 mm Hg for men separately [14].

IOP for women and men is comparative within the same age group, while IOP in earlier age is greater when contrasted with older-age groups. For diabetic populace, the mean IOP was 15.08 ± 2.18 mm Hg.

Spherical Equivalent (SE)=Sphere Power+1/2(Cylinder Power)   (1)

With a spectacle amendment of -3.01 +1.01 x 180, the SE = -3.00D + ½(+1.00D) = -3.00D + 0.50D = -2.50D. Nearsightedness has been characterized using SE as ≤−0.50 diopters (D); mellow nearsightedness is characterized as ⟩−3.0 D; moderate nearsightedness is characterized as ≤−3.0D; and high nearsightedness is characterized as ≤−6.0D. Mean IOP has been found that 15.98 mmHg in

typical hyperopic eyes and ultimately raised with myopia progression to 16.2 mmHg. The table 4. below lists the normal and abnormal eyes in relation to refractive errors and IOP.

Table 4. Normal and POAG Mean IOP related to RE

	Normal		POAG	
	Mean IOP (mmHg)	N	Mean IOP (mmHg)	N
SE ≤−0.50 D (Myopia)	15.6	1823	23.6	167
SE >−3.0 D (Slight Myopia)	15.9	1526	21.3	256
SE ≤−3.0 D (Moderate Myopia)	16.4	532	22.1	92
SE ≤−6.0 D (High Myopia)	16.9	425	21.2	45

As a result, analysis of this massive population-based study revealed that the occurrence of glaucoma is strongly influenced by RE and manifested in bigoted eyes. Eyes with low IOP have a stronger link to glaucoma than eyes with the middle pressure tests, which have a weaker link, and eyes with excessive pressure have no link at all.

5. CONCLUSION

Populace based health examination and has been directed for analyzing diabetes retinopathy in India. Increasingly serious nearsightedness was related with a more prominent probability of glaucoma in a Wheatish population matured forty and further years. This constructive connection among the RE and IOP underlines the significance of glaucoma observation in the nearsighted populace in light of the fact, that both raised IOP and nearsightedness are significant hazard factors for glaucoma development. This paper demonstrates that, there is a solid association among RE, IOP, visual biometry and POAG for diabetes more protuberant than 40 years in Wheatish populace. The incorrected RE can be rectified with eyeglasses while cataracts medical procedure can reestablish image. Vision recovery is additionally powerful in enlightening irretrievable vision debilitation. Here a deep learning algorithm is developed to detect the severity of glaucoma in diabetic patients with the fundus image. In this study, it is found that, the individual group with the age of 60-69 are more affected by glaucoma with 65.89% of PACG, 62.50% of POAG, 62.25% of NTG, 45.95% of PIGM and 51.69% of OH among Wheatish population. Curiously the relationship among refractive error and IOP varied by age group, yet IOP was unequivocally connected with glaucoma and refractive error for diabetes.

CONFLICTS OF INTEREST

The authors affirm the fact that there are no known conflicts of interest that might have seemed to an impact on the research presented in this study.

REFERENCES

[1] H. Choquet, J. L. Wiggs, J. L. and A.P. Khawaja, "Clinical implications of recent advances in primary open-angle glaucoma genetics", *Eye*, vol. 34, no.1, pp.29-39, 2020. [CrossRef] [Google Scholar] [Publisher Link]

[2] S. Resnikoff, D. Pascolini, D. Etya'ale, I. Kocur, R. Pararajasegaram and G. P. Pokharel, "Global data on visual impairment in the year 2002", *Bull World Health Organ* vol. 82, pp. 844-51, 2004. [CrossRef] [Google Scholar] [Publisher Link]

[3] C.F.M. Vasconcelos, V.T. Ribas, and H. Petrs-Silva, Shared Molecular Pathways in Glaucoma and Other Neurodegenerative Diseases: Insights from RNA-Seq Analysis and miRNA Regulation for Promising Therapeutic Avenues. Cells, vol. 12, no. 17, p.2155, 2023. [CrossRef] [Google Scholar] [Publisher Link]

[4] M.I. Mokbul, Optical Coherence Tomography Angiography (OCT-A): Emerging Landscapes in Neuro-Ophthalmology and Central Nervous System (CNS) Disorders, 2023. [CrossRef] [Google Scholar] [Publisher Link]

[5] M.M. Hasan, J. Phu, A. Sowmya, E. Meijering, and M. Kalloniatis, Artificial intelligence in the diagnosis of glaucoma and neurodegenerative diseases. Clinical and Experimental Optometry, pp.1-17, 2023. [CrossRef] [Google Scholar] [Publisher Link]

[6] R. George R, S. Ramesh, and L. Viajaya "Glaucoma in India: Estimated burden of disease", *J Glaucoma*, vol.19, pp. 391-97, 2010. [CrossRef] [Google Scholar] [Publisher Link]

[7] S. Diaz-Torres, W. He, J. Thorp, S. Seddighi, S. Mullany, C.J. Hammond, P.G. Hysi, L.R. Pasquale, A.P. Khawaja, A.W. Hewitt, and J.E. Craig, Disentangling the genetic overlap and causal relationships between primary open-angle glaucoma, brain morphology and four major neurodegenerative disorders. EBioMedicine, 92, 2023. [CrossRef] [Google Scholar] [Publisher Link]

[8] A. Hakim, B. Guido, L. Narsineni, D.W. Chen, and M. Foldvari, Gene therapy strategies for glaucoma from IOP reduction to retinal neuroprotection: progress towards non-viral systems. Advanced Drug Delivery Reviews, p.114781, 2023. [CrossRef] [Google Scholar] [Publisher Link]

[9] A. Bali, and V. Mansotra, Analysis of Deep Learning Techniques for Prediction of Eye Diseases: A Systematic Review. Archives of Computational Methods in Engineering, pp.1-34, 2023. [CrossRef] [Google Scholar] [Publisher Link]

[10] H. Yokomichi, K. Kashiwagi, K. Kitamura, Evaluation of the associations between changes in intraocular pressure and metabolic syndrome parameters: a retrospective cohort study in Japan. *BMJ Open,* vol. 6, pp. e010360, 2016. [CrossRef] [Google Scholar] [Publisher Link]

[11] H.D. Jang, D.H. Kim, and K. Han, Relationship between intraocular pressure and parameters of obesity in Korean adults: the 2008–2010 Korea National Health and Nutrition Examination Survey. *Curer Eye Res* 2015; 40: 1008–17. [CrossRef] [Google Scholar] [Publisher Link]

[12] Ling Shen, The Association of Refractive Error with Glaucoma in a Multiethnic Population, *Ophthalmology,* pp. 1-10, 2015. [CrossRef] [Google Scholar] [Publisher Link]

[13] Tien Yin, Glaucoma in a white population, *American academy of ophthalmology,* pp 211-217, 2003. [CrossRef] [Google Scholar] [Publisher Link]

[14] Sudarshan Khokhar et al., refractive outcomes of cataract surgery in primary congenital glaucoma, *eye,* 2018. [CrossRef] [Google Scholar] [Publisher Link]

[15] M.S. Tedja, R. Wojciechowski, P.G. Hysi, Genome-wide association meta-analysis highlights light-induced signaling as a driver for refractive error. *Nat Genet.* Vol. 50, pp. 834–848, 2018. [CrossRef] [Google Scholar] [Publisher Link]

[16] G. Thorleifsson, G.B. Walters, A.W. Hewitt, Common variants near CAV1 and CAV2 are associated with primary open-angle glaucoma. *Nat Genet.* Vol. 42, pp.906–909, 2010. [CrossRef] [Google Scholar] [Publisher Link]

[17] T.Y. Wong, B.E. Klein, R. Klein, M. Knudtson, and K.E. Lee, Refractive errors, intraocular pressure, and glaucoma in a white population. *Ophthalmology,* vol.110, no. 1, pp.211-217, 2003. [CrossRef] [Google Scholar] [Publisher Link]

[18] A.V. Varadarajan, R. Poplin, K. Blumer, C. Angermueller, J. Ledsam, R. Chopra, P.A. Keane, G.S. Corrado, L. Peng, and D.R. Webster, Deep learning for predicting refractive error from retinal fundus images. *Investigative ophthalmology & visual science,* vol. 59, no. 7, pp. 2861-2868, 2018. [CrossRef] [Google Scholar] [Publisher Link]

[19] R. Sihota, D. Angmo, D. Ramaswamy, and T. Dada, Simplifying "target" intraocular pressure for different stages of primary open-angle glaucoma and primary angle-closure glaucoma. *Indian journal of ophthalmology,* vol. 66, no. 4, p.495, 2018. [CrossRef] [Google Scholar] [Publisher Link]

[20] L.G.M. Pimentel, C.P. Gracitelli, L.S.A.C. da Silva, A.K.S. Souza, and T.S. Prata, Association between glucose levels and intraocular pressure: pre-and postprandial analysis in diabetic and nondiabetic patients. *Journal of ophthalmology,* 2015. [CrossRef] [Google Scholar] [Publisher Link]

[21] N. Singh, L. Kaur, and K. Singh, Histogram equalization techniques for enhancement of low radiance retinal images for early detection of diabetic retinopathy. *Engineering Science and Technology, an International Journal,* vol. 22, no. 3, pp.736-745, 2019. [CrossRef] [Google Scholar] [Publisher Link]

[22] M.Y. Yip, G. Lim, Z.W. Lim, Q.D. Nguyen, C.C. Chong, M. Yu, V. Bellemo, Y. Xie, X.Q. Lee, H. Hamzah, and J. Ho, Technical and imaging factors influencing performance of deep learning systems for diabetic retinopathy. *NPJ digital medicine, vol.* 3, no.1, pp.1-12, 2020. [CrossRef] [Google Scholar] [Publisher Link]

[23] D.S. Sisodia, S. Nair, and P. Khobragade, Diabetic retinal fundus images: Preprocessing and feature extraction for early detection of diabetic retinopathy. *Biomedical and Pharmacology Journal,* vol. 10, no. 2, pp.615-626, 2017. [CrossRef] [Google Scholar] [Publisher Link]

AUTHORS

Dr. A. PRASANTH received the B.E. degree in Electronics and Communication Engineering from Anna University, Chennai and the M.E degree in Computer Science and Engineering (with specialization in Networks) from Anna University, Chennai and also received the Ph. D degree in Information and Communication Engineering from Anna University, Chennai, India. He is currently working as an Assistant Professor at Sri Venkateswara College of Engineering, Sriperumpudur, Tamilnadu, India. He has published more than 35 research articles in reputed International Journals among which 10 articles are indexed in SCI and 15 articles are indexed in Scopus. He has published 4 patents in IPR cell. Further, he has published more than 8 Books under reputed publisher. He has served as Resource person in 25 AICTE Sponsored STTP/FDP programs. Moreover, he has served as Editorial Board Member in various reputed SCI Journals. His research interests include Internet of Things, Blockchain, Wireless Sensor Networks, Medical Image Processing, and Machine Learning.

Dr. N. Muthukumaran was born in Kaniyakumari, Tamilnadu, India, in 1984. He received the B.E Degree in Electronics and Communication Engineering, M.E Degree in Applied Electronics and the Ph.D Degree in Information and Communication Engineering from Anna University, Chennai, India in 2007, 2010 and 2015 respectively. He is currently working as a Professor & Research centre lab, Department of Electronics and Communication Engineering in Francis Xavier Engineering College, Affiliated to Anna University Chennai, Tirunelveli, Tamilnadu, India. His major research interests are in the field of Digital Image/ Signal Processing, Multimedia Image/ Video Processing/ Compression, Digital and Analog Very Large Scale Integration circuit design. Since 2006 he has published more than 73 International Journals like Springer, IEEE, Elsevier and 88 National/International conferences papers. He has published 15 International Books which is related to Engineering Students and 27 Innovation Patents. He has actively participate and organized more than 102 research related events like National and International Workshop, Faculty Development Program, Seminar, Symposium, Conference and Short Term Courses Delivered & Attended. He has collaborated and life time member of more than 19 various Memberships body Association like IEEE, ISI, WCECS, UACEE ect.